TELEOPERATED MOTION SCALING ROBOTIC MANIPULATOR WITH FORCE FEEDBACK

A Thesis
Presented to
The Academic Faculty

by

Yongmin Cho

In Partial Fulfillment
of the Requirements for the Degree
Master of Science in the
George W. Woodruff School of Mechanical Engineering

Georgia Institute of Technology
May 2020

TELEOPERATED MOTION SCALING ROBOTIC MANIPULATOR

WITH FORCE FEEDBACK

Approved by:

Dr. Frank Hammond III, Advisor
School of Mechanical/Biomedical Engineering
Georgia Institute of Technology

Dr. Jun Ueda
School of Mechanical Engineering
Georgia Institute of Technology

Dr. Jaydev P. Desai
School of Mechanical Engineering
Georgia Institute of Technology

Date Approved: [April 21, 2020]

To my wife,

Yoonji

ACKNOWLEDGEMENTS

I wish to express my deepest gratitude to my thesis advisor Dr. Frank L. Hammond III of the School of Mechanical/Biomedical Engineering at Georgia Institute of Technology. He offered warm encouragement and continuous support throughout my master's program. He also provided valuable guidance and made sure that I was on the right track towards my research goal. He has been greatly helpful to me throughout the years at Georgia Tech.

I also would like to extend my appreciation to Dr. Jun Ueda and Dr. Jaydev P. Desai for being my committee members. I am greatly enlightened by their insightful questions and valuable suggestions for the improvement of my thesis. I would like to thank Lasitha Wijayarathne for his advice on the control algorithm. I also thank Bryan Blaise for his assistance in the initial setting of the Phantom Omni.

Finally, my special thanks goes to my wife, Yoonji, for her sincere care and continuous help. Without her heartwarming love and sacrifices, this work would not have been possible, and I owe all my achievements to her. I would also like to thank my parents, parents-in-law, Ara Cho, and Kyongnam Noh who have been greatly supportive and encouraged me throughout the years at Georgia Tech

TABLE OF CONTENTS

LIST OF TABLES

LIST OF FIGURES

LIST OF SYMBOLS AND ABBREVIATIONS

TMSRA	Teleoperated Motion Scaling Robotic Arm
OSHA	Occupational Safety & Health Administration
DOF	Degree of Freedom
DH parameters	Denavit–Hartenberg parameters
ROS	Robot Operating System

SUMMARY

The demand for construction work from new residential construction and new non-residential construction has been increased. A major reason for the high demand for construction and heavy equipment is due to rising construction activities, an increase in government investment due to rising in the residential sector, and urbanization and economic growth. Additionally, many older buildings have been demolished, and new high-rise buildings have been built due to land shortages in highly populated cities.

On construction sites, there are roughly 150,000 accidents every year in the U.S., and these accidents range from small accidents to casualties. The causes of accidents involve many factors, including falls, impacts by objects, electrocution, and being caught in machinery. Additionally, excavating near buried facilities is statistically one of the main causes of accidents. For example, the excavating could cause an explosion by damaging a buried gas pipe when performing excavating tasks on construction sites.

Based on the background information, there is a clear need for more efficient construction methods because of higher demand and a shortage of equipment operators. Also, there is a need for safer construction equipment to reduce accidents on construction sites. The teleoperation of construction equipment could help to avoid casualties because human operators do not have to be in the construction equipment during its use. Teleoperation also prevents exposure to typical construction dust, including silica dust that causes silicosis, lung cancer, and other respiratory diseases. Additionally, adopting force feedback to the teleoperated construction equipment could decrease accidents from damaging undergrounded utilities, such as water and sewer pipes, power cables, natural gas lines, etc. by recognizing the impact well. Teleoperated motion scaling construction

equipment will possibly improve the efficiency of construction work. The addition of motion scaling to the heavy construction equipment provides not only the efficient control of the equipment but also the dexterous control of the equipment.

This study introduces a Teleoperated Motion Scaling Robotic Arm (TMSRA) platform that allows the human operator to control the motion-mapping rate between the master (haptic console) and slave (robotic excavator) devices, while also providing force feedback and virtual safety functions to help prevent excessive force application by the slave device. This study experimentally evaluated the impact of motion scaling and force feedback on human users' ability to perform simulated construction tasks. Experimental results from simulated robotic excavating and demolition tasks show that the maximum force applied to fictive buried facilities was reduced by 77.67% and 76.36% respectively due to the force feedback and safety function. Experimental results from simulated payload pushing/sliding tasks demonstrate that the provision of user-controlled motion scaling increases task efficiency, reducing completion times by at least 31.41%, and as much as 47.76%.

CHAPTER 1. **INTRODUCTION**

According to the Bureau of Labor Statistics, the demand for construction equipment operators will grow 10 percent from 2018 to 2028 because spending in infrastructure is expected to increase [1]. Statista, a German online portal for statistics, reported that private construction spending in the U.S. reached around 992 billion USD in 2018. They predict that new construction spending reaches over 1.45 trillion USD by 2023, new non-residential construction spending reaches over 562 billion USD, and new residential construction spending reaches over 527 billion USD by 2020 [2]. Large construction projects across asset classes typically take 20 percent longer to finish than scheduled and are up to 80 percent over budget [3]. Because of higher demand and shortage of equipment operators, there is a need for more efficiency of construction work.

According to the Bureau of Labor Statistics, there are around 150,000 construction site accident injuries every year. Although there are many safety precautions, such as soil classification, fall protection needs, surface and groundwater, the water table location, and underground utilities, mandated by OSHA to protect workers on construction sites, accidents can still take workers' lives. According to the 2018 Damage Information Reporting Tool (DIRT) report [4] by Common Ground Alliance, which describes gathered data regarding damage and unplanned events from excavation tasks related to buried facilities, the estimated number of total damages in the U.S. increased from 439,000 in 2017 to 509,000 in 2018. Besides accidents on construction sites, construction activities generate dust that can cause respiratory dysfunctions [5-7]. According to the Health and Safety Executive (HSE) in the United Kingdom, over 500 construction workers are believed to die from exposure to silica dust every year [8].

1.1 Motivation 1: High Demand of New Construction

Figure 1 shows that construction spending in the United States was around 788 billion USD in 2011 when construction spending reached the lowest level in a decade. However, new construction spending in the United States was valued at around 1.29 trillion USD in 2018, and the industry is expected to generate around 1.45 trillion USD in revenue by 2023. This data shows that the construction industry is on track to continue its growth trend.

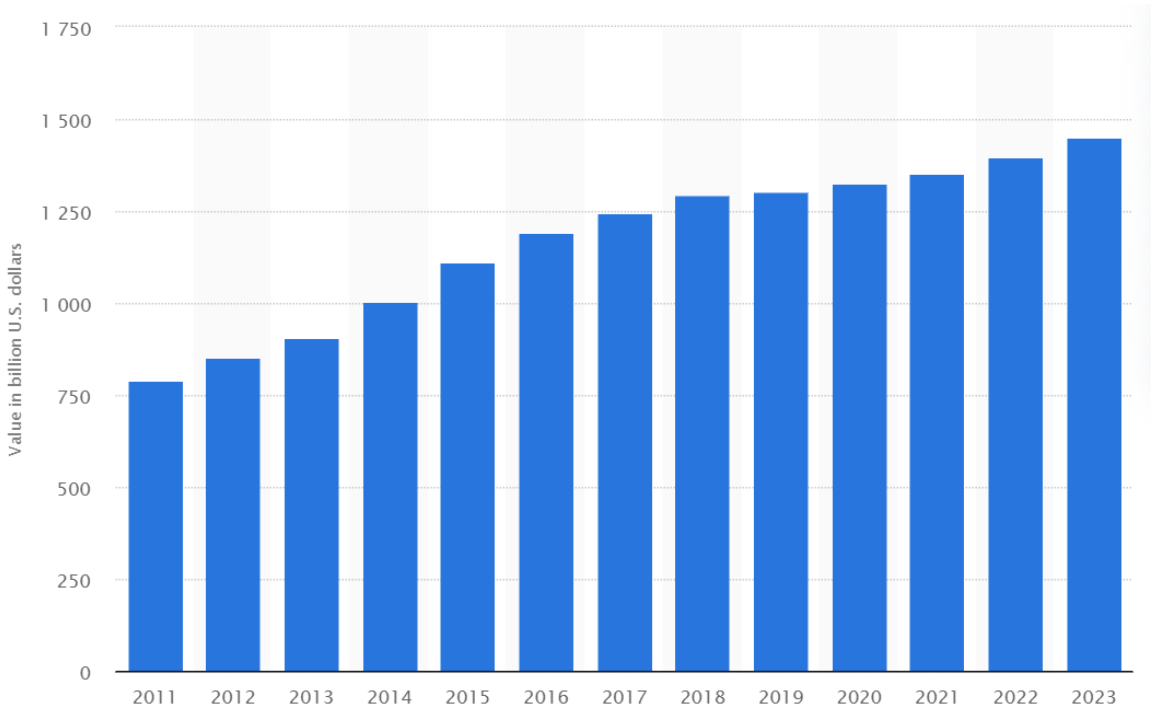

Figure 1 - Forecast for New Construction in the U.S. [9]

1.2 Motivation 2: Causes of Accidents on Construction Sites

There are many direct or indirect causes of accidents on construction sites such as falls, impacts by objects, electrocutions, machinery catching workers, etc., so it is important to identify the root causes to prevent accidents. According to the DIRT report [4] as seen in Figure 2, 'No notification made to One-Call Center/811' had the largest portion of root cause and it was followed by 'Improper excavation practice', 'Excavator dug prior to verifying marks by test-hole', and 'Excavator dug prior to valid start date/time'.

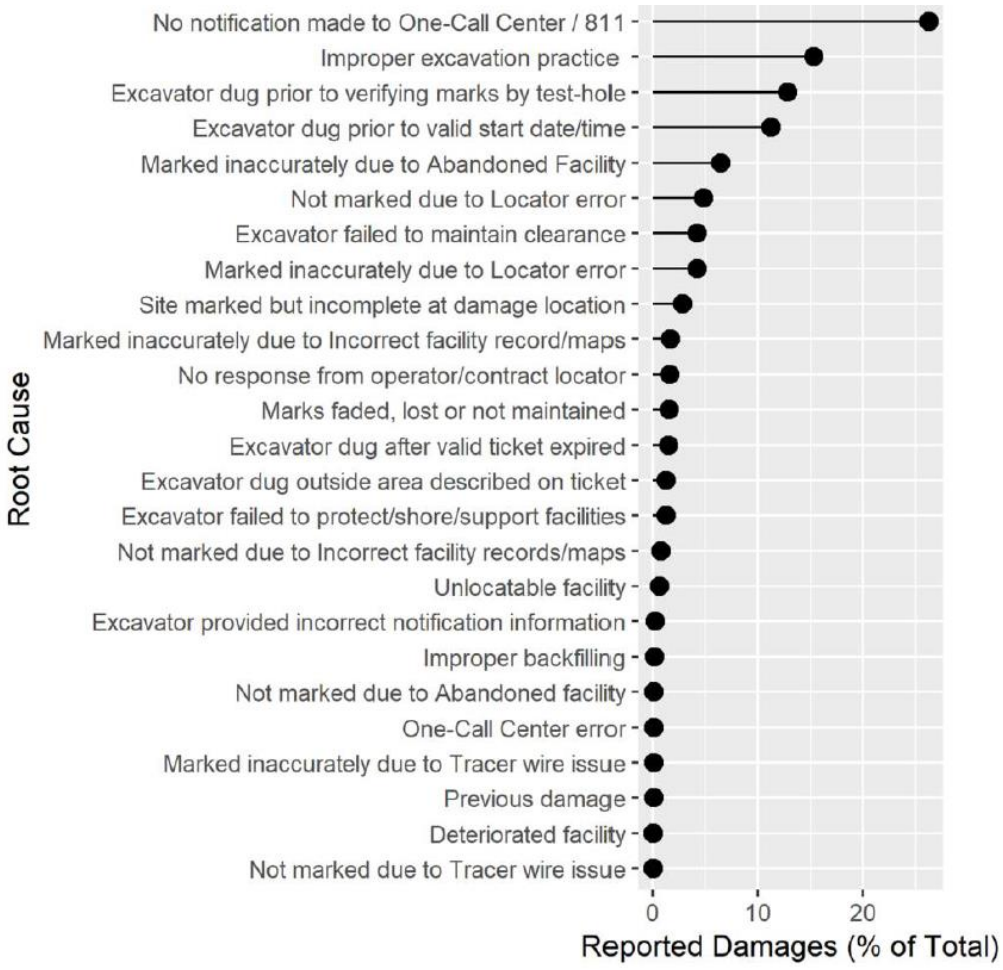

Figure 2 - Reported damaged by root cause in Canada and the U.S., 2018 [4]

Figure 3 shows root cause groupings by the DIRT report [4], and the 'Excavating Issue' was the largest part of root cause groups in both 2017 and 2018. Once construction is determined and needs excavation for the construction, a notice of intent to dig must be made to a local call center. 'Notification Not Made' represents damages caused by this step not being followed. After the notice, the facility operator or contractor must mark the location of the buried facilities accurately and timely. 'Locating Issue' captures damages where this did not happen. After those two steps, careful excavating must be performed when digging near buried facilities. 'Excavation Issue' captures damages where something went wrong here. 'Other Notification Issue' on Figure 3 represents situations where an 811 notification was made but something about it was invalid. 'Miscellaneous' represents damages causes that do not fit well into a notification, locating, or excavating category. Lastly, 'Unknown/Other' captures damages where the root cause was not collected or none of the available choices fit.

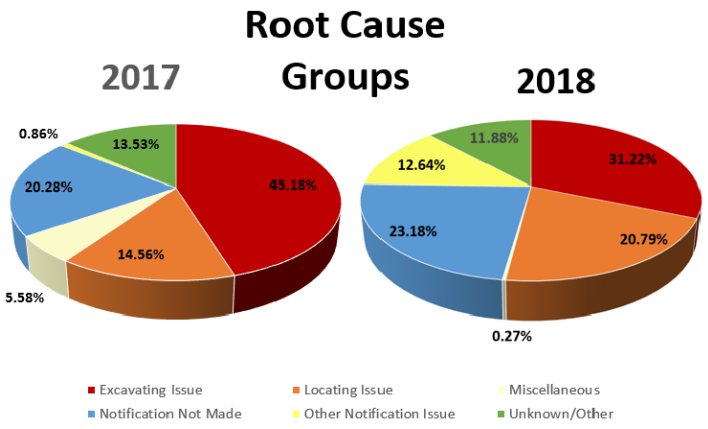

Figure 3 - Root cause groupings for 2017 and 2018 [4]

According to Figures 2 and 3, 'Excavating Issue' is taking large portions of both root cause and root cause groups, and only 'Excavating Issue' is directly linked to an accident, so it is important to have a solution to reduce the excavating issue.

1.3 Motivation 3: Dust on Construction Sites

On construction sites, there are three major types of dust. First, silica dust is created when working on materials, such as soil, sand, granite, stone, brick, and concrete. Second, wood dust is created from various types of wood, such as softwood, hardwood and wood-based products like medium-density fiberboard and plywood. Last, lower toxicity dust is created when working on materials that involve gypsum, limestone, marble, and dolomite. Additionally, respirable dust generated in construction activities, such as crystalline silica and particulates not otherwise specified, causes depressed lung function. Therefore, construction workers can be classified as a high-risk group for respiratory diseases [10]. According to the OSHA [11], crystalline silica has been classified as a human lung carcinogen. Inhalation of crystalline silica dust can cause silicosis, which in severe cases can be disabling, or even fatal and there is no cure for silicosis. Based on the above information, the construction workers should be protected from the construction dust for their health.

1.4 Potential of Teleoperation with Force Feedback on Construction Sites

Construction is one of the largest industries in the world, yet also one of the slowest to adopt new technology due, in large part, to the prohibitive costs of upgrading heavy equipment [12]. However, as global construction demands continue to increase rapidly, the industry faces a number of logistical challenges that may only be solvable by the adoption of new technology. One of the challenges is equipment transportation and maintenance. The relocation and upkeep of heavy machinery across multiple construction sites are time consuming and expensive, from an operations management perspective. Another challenge

is a shortage of skilled human capital. Construction bandwidth is limited by the availability of experienced workers, forcing large delays in projects and reducing profits. One continuing challenge is safety in the austere construction environment. New construction methods enable more ambitious development projects (i.e. larger buildings and more complex environments) but can also increase risks to workers.

These issues have motivated a strong interest in the development of teleoperated construction equipment aimed at improving worker safety, worksite accessibility, and operational efficiency for global construction companies.

There are many efforts in teleoperated construction using excavators to address challenges on construction sites. Since 1990, various studies focused on the topic of teleoperated excavators have been conducted [16]-[20]. Teleoperated excavators with virtual reality technology were developed and implemented to improve task efficiency and user control with a visual display consisting of graphical images [21]-[23]. Studies were conducted in which force feedback was provided to excavator teleoperators for improved contact sensing [24],[25]. The master systems in these studies were good to apply directly to the conventional excavators because they use lever-type joysticks. Conventional hydraulic joysticks were replaced with several haptic devices to improve the control efficiency of unskilled operators [26],[27]. The new haptic devices from these studies lowered the barrier to entry because the haptic devices allowed for operators to get used to the manipulation method more easily. However, the previous studies did not include the motion scaling teleoperation to control the excavators strategically to improve task efficiency.

This study introduces a novel system, a Teleoperated Motion Scaling Robotic Arm

(TMSRA), which has the potential to significantly improve the control efficiency of teleoperated robotic manipulators, like excavators, by using human-friendly haptic devices and motion scaling. With the scaled motion, the teleoperated robot can reach the different points in the workspace quickly, but also move slowly and more precisely to avoid unexpected damage to objects, which should not be impaired. This system also reduces the maximum forces on buried fictive objects representative of water and sewer pipes, power cables, and natural gas lines by providing force feedback. It could potentially reduce accidents in a real-world application.

1.5 Thesis Outline

Chapter 2 introduces the overall design of TMSRA. First, it describes how the configuration of the physical robotic arm was determined and what types of end-effectors the robotic arm had for this study. Second, the design of the physical robotic arm as a slave robot system is introduced, such as the length of links and the number of actuators. Also, a haptic device as a master system that controlled the slave robot system is introduced. Last, the overall control algorithm to control actuators and the haptic device for the TMSRA with force feedback is introduced.

Chapter 3 describes the motion-scaling teleoperation for the physical robotic arm. A velocity control algorithm between the robotic arm and the haptic device that implemented both micro-teleoperation and macro-teleoperation is introduced. Furthermore, this chapter shows the experimental results to show the effect of motion scaling teleoperation.

Chapter 4 describes how paring the TMSRA with force feedback and a safety function reduces the maximum forces on buried objects. Moreover, the experimental result shows a stark difference between the TMSRA with and without the force feedback.

Chapter 5 reflects on the full scope of research conducted in this investigation. It describes general observations on the performance of tested systems and aspects to improve the system. Additionally, an aim for future work is given to improve work efficiency and have a more reliable system.

CHAPTER 2. DESIGN OF TELEOPERATED MOTION SCALING ROBOTIC ARM (TMSRA)

The term teleoperation can be defined as the operation of a system remotely located from the user [28]. Because a system is remotely controlled, teleoperation is well known for its important role in manipulating remote objects using a robotic arm especially in a hazardous environment [29]. Teleoperation has been used in different applications, such as surgical robotics [30], space robotics [31], search and rescue in disaster sites [32], disarming of explosives [33] and nuclear or chemical industry [34]. In the field of surgical robotics, the motion scaling teleoperation is widely used to enable the clinician to intuitively and accurately control the motion of the slave end-effector [30]. The workspace is very limited, so the motion of the slave robot is scaled down. When adopting the motion scaling teleoperation to construction sites, both increased and decreased motion scaling should be used. Thus, the robot can reach different points in the workspaces quickly using increased motion scaling as well as move slowly and more precisely using decreased motion scaling to improve the efficiency and quality of work.

2.1 Types of Construction Heavy Equipment and Attachments of the Excavator

These days, many types of construction heavy equipment are observed around easily in daily life. Construction heavy equipment is used for various purposes, such as paving a road, building houses, etc. in large projects. The types of construction equipment include excavators, backhoe, dragline excavator, bulldozers, graders, wheel tractor scraper, trenchers, loaders, cranes, pavers, compactors, telehandlers, feller bunchers, dump trucks, pile boring machine, and pile driving machine. For paving a road, the main types of

construction equipment are pavers and compactors. In the case of building construction, heavy equipment, such as excavators, cranes, and telehandlers, are chiefly used.

For this study, the configuration of an excavator (Figure 4) was chosen to test the TMSRA with force feedback because excavators were the most commonly used equipment on construction sites so that the result of this research could give more contribution to the construction industry. Another reason for the choice was that excavators were more functional than other types of construction heavy equipment. By simply changing the attachment of the excavators, an excavator can perform multiple tasks, such as digging, demolition, and compaction tasks so that this study could more contribute to the construction industry no matter what the tasks are.

Figure 4 - Caterpillar Small Excavator 311F L RR [35]

Excavators are capable of using the various attachment as shown in Figure 5. With these types of attachment, excavators play an important role in construction sites. For this study, a digging bucket and ripper were chosen to test the TMSRA because digging and demolition tasks were the representative tasks on construction sites and the mechanism to control both types of attachment is the same so that it was easy to test different tasks with a control mechanism.

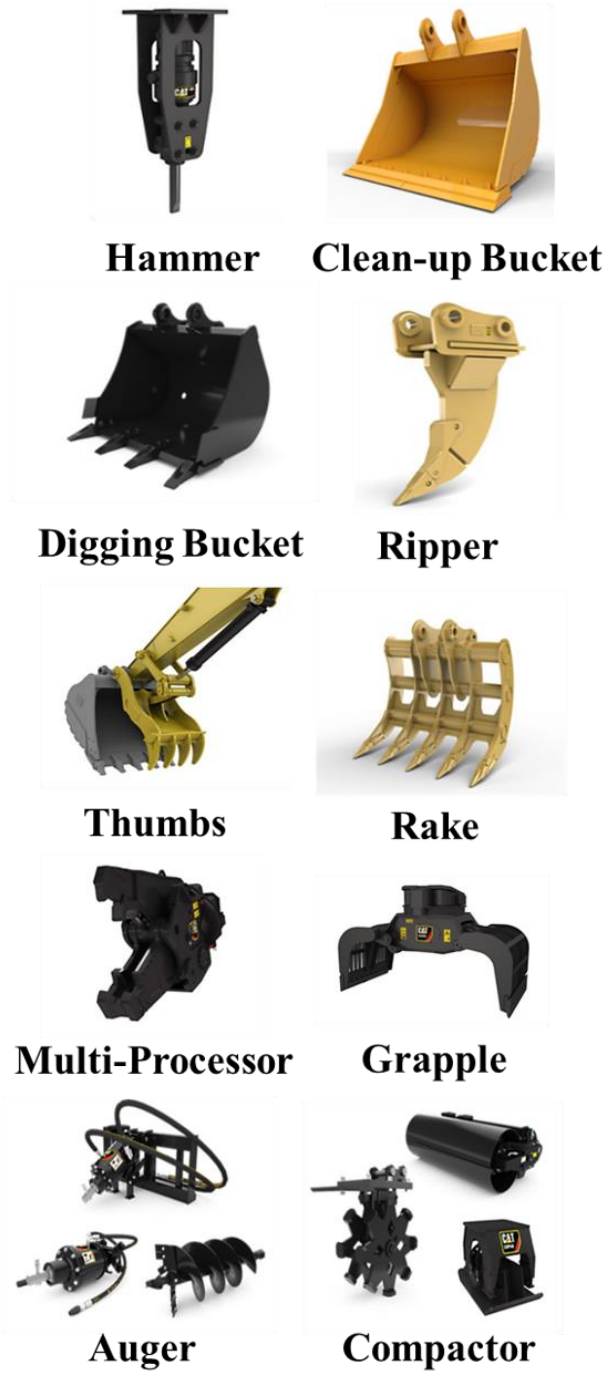

Figure 5 - Excavator Attachments [36]

2.2 Slave Robot System

2.2.1 Comparison to the Conventional Excavator

As described in Section 2.2, the configuration of an excavator was selected to test the TMSRA with force feedback in this study, so the slave robot system replicated an excavator seen in Figure 4. The conventional excavator was too big to perform an experiment in an indoor lab, so the physical robotic arm was scaled down from a conventional excavator, the Caterpillar 323F L Hydraulic Excavator (Figure 6). This hydraulic excavator's boom length was 5080 mm and the length of the boom on the physical robotic arm was 112.3 mm (Figure 7). The physical robotic arm was scaled down based on the length of the booms, and the reduction ratio was approximately 45:1. The reduction ratio was to match the dimensions of the physical robotic arm with the dimensions of a master system approximately to improve the operators' intuitive. Detailed dimensions for the physical robotic arm are shown in Figure 7.

Most conventional excavators use a hydraulic valve system to move the excavator's boom, arm, and attachment, but this study used servo motors for the physical robotic arm to make it simpler and to have better position control. The swing drive and motor' on the excavator (Figure 6) rotate the upper part of the excavator, involving the boom, stick, and bucket. The boom cylinder is responsible for moving the boom upward and downward. Similarly, the stick cylinder changes the position of the stick upward and downward. Lastly, the orientation of the bucket is changed by the bucket cylinder, so the bucket cylinder opens or closes the bucket.

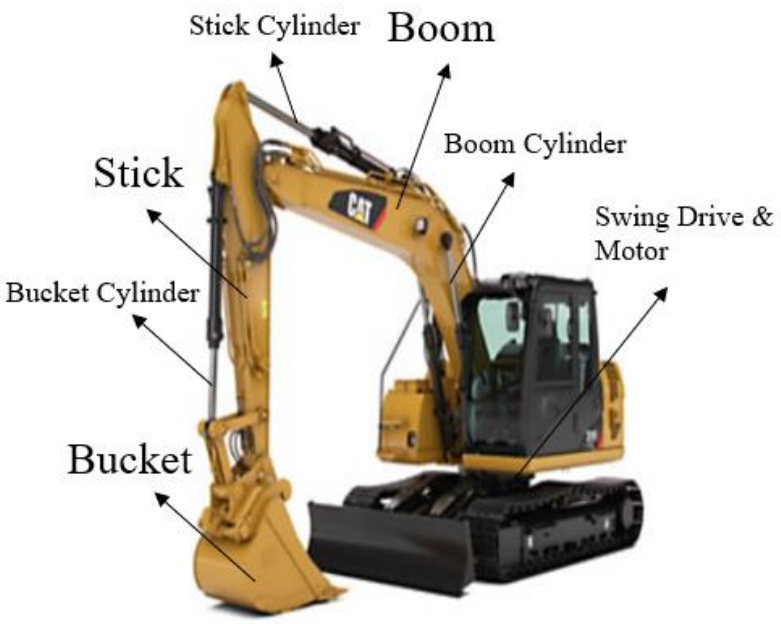

Figure 6 - Caterpillar Small Excavator 311F L RR with Part Name [35]

The slave robotic arm was based on a serial architecture with four revolute joints in Figures 7 and 8. It had a 3D-printed base part for an actuator to rotate the upper part of the robotic arm and a rotational turntable supported the upper part of the robotic arm. Joint hinges for the upper three actuators were obtained from ROBOTIS and all other parts for the physical robotic arm were 3D-printed or laser-cut. The slave system was composed of an ATI Nano17 sensor mounted between an end-effector and the distal motor. The Nano17 sensor was a six-axis force/torque sensor to sense force information of the end-effector when performing tasks. As described above in Section 2.2, a bucket and ripper were selected as end-effector for the slave robotic arm.

Below, Figures 7 and 8 show the physical robotic arm designed in SolidWorks. Similar to the conventional excavator, the robotic arm consists of four revolute joints, which mimic the movement of the excavator. The role of motor 1 in Figure 7 is the same as the swing drive and motor on the excavator in Figure 6. This motor revolves along the

Z-axis in Figure 7 and rotates the upper parts, involving motor 2, motor 3, motor 4, bucket, and links between each motor and the bucket in Figure 7. The role of motor 2 and motor 3 in Figure 7 is the same as the boom cylinder and stick cylinder in Figure 6. Like the bucket cylinder in Figure 6, Motor 4 in Figure 7 is opening and closing the bucket for digging tasks. For Figure 8, everything is the same as Figure 7, but the bucket is replaced with a ripper for the demolition task. The slave robotic arm with the bucket could reach up to 371.68 mm in the x-axis and y-axis and 533.14 mm in the z-axis.

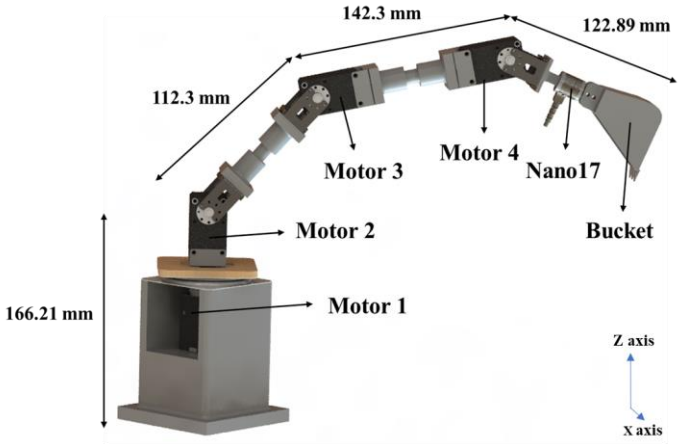

Figure 7 - Physical Robotic Arm with a Bucket with dimensions

Figure 8 - Physical Robotic Arm with a Ripper

2.2.2 Inverse Dynamics for Motor Selection

To select the proper motors, it was essential to know the required joint torques to move the physical robotic arm from a position to other positions. Inverse dynamics calculated the required joint torques when external forces applied to a rigid body [37], [38]. In this study, DH parameters [37] were developed first. Then, the inverse dynamics were calculated by using the DH parameters and a robotics toolbox for MATLAB by Peter Corke [39]. Table 1 shows the DH parameters of the physical robotic arm. In the table, a_{i-1} represents the distance from $\hat{Z}_i$ to $\hat{Z}_{i+1}$ measured along $\hat{X}_i$. and α_{i-1} corresponds to the angle between $\hat{Z}_i$ and $\hat{Z}_{i+1}$ measured about $\hat{X}_i$. In addition, d_i represents the distance from $\hat{X}_{i-1}$ to $\hat{X}_i$ measured along $\hat{Z}_i$ and θ_i corresponds to the angle between $\hat{X}_{i-1}$ and $\hat{X}_i$ measured about $\hat{Z}_i$.

Table 1 - DH Parameters of the Physical Robotic Arm

i	a_{i-1}	α_{i-1}	d_i	θ_i
1	0	0	0	θ_1
2	0	$\frac{\pi}{2}$	0.16621	θ_2
3	0.1123	0	0	θ_3
4	0.1423	0	0	θ_4

Figure 9 shows the physical robotic arm configuration in MATLAB with 0 for θ values based on the DH parameters in Table 1. The pair of blue, green, and red lines represent a configuration of a joint. Here, the blue lines represent the axis of rotation of the motors. The green lines and red lines represent the direction of the y-axis and the x-axis

for each joint, respectively. From the calculations for the inverse dynamics on MATLAB by the robotics toolbox, the minimum joint torques for the physical robotic arm to hold the configuration like Figure 9 were 0, 0.48 Nm, 0.3340 Nm, and 0.072 Nm, respectively. Based on the calculation and consideration of additional external forces for tasks with a bucket and a ripper, two kinds of servo motors were selected for the physical robotic arm. One was XM540-W150-R (165 g) by ROBOTIS and the other one was XM430-W210-R (82 g) by ROBOTIS. The former servo motor was used for the base to rotate the whole robotic arm and the latter servo motors were used for all other joints. The stall torque of the former was 7.3 Nm at 12 V and the stall torque of the latter was 3.0 Nm at 12 V. These torque values were enough to move the robotic arm to the desired position even with some external forces were applied to the end-effector.

Previously, the physical robotic arm was designed with four DC motors, but it was changed to Dynamixel servo motors by ROBOTIS because of backlash, weight, and resolution. The selected servo motors had many advantages compared to the previous DC motors such as modularity, serial chaining, integrated controller, six operating modes, higher resolution, and smaller backlash, and lighter weight.

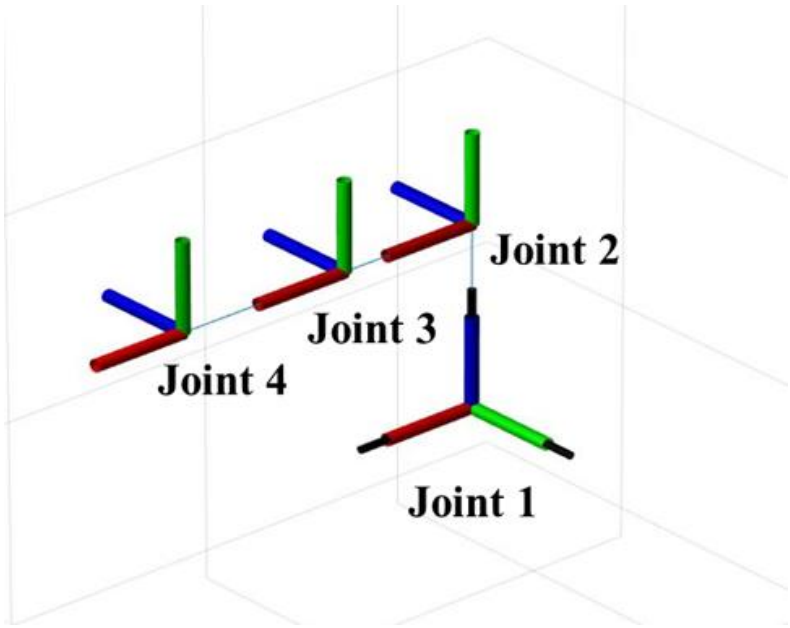

Figure 9 - Physical Robotic Arm Configuration with 0 for θ values

2.2.3 Kinematics model

The DH parameters for the physical robotic arm in Table 1 are then used to compute the homogeneous transformation matrices, ${}^{0}_{4}T$.

$$ {}^{0}_{4}T = \begin{bmatrix} C_1C_{23} & -C_1S_{23} & S_1 & C_1C_{23}L_3 + C_1C_2L_2 \\ S_1C_{23} & -S_1S_{23} & -C_1 & S_1C_{23}L_3 + S_1C_2L_2 \\ S_{23} & C_{23} & 0 & S_{23}L_3 + S_2L_2 + L_1 \\ 0 & 0 & 0 & 1 \end{bmatrix} $$

Where C_1 represents cos (θ_1), C_{23} represents cos $(\theta_2 + \theta_3)$, L_1 is 166.21 mm, L_2 is 11.23 mm, and L_3 is 14.23mm.

The first three entries of the last column in ${}^{0}_{4}T$ represent the position of the end-effector in Cartesian coordinates with respect to the base of the physical robotic arm.

$$x = C_1C_{23}L_3 + C_1C_2L_2 \quad (1)$$

$$y = S_1C_{23}L_3 + S_1C_2L_2 \quad (2)$$

$$z = S_{23}L_3 + S_2L_2 + L_1 \quad (3)$$

For the inverse kinematics, the position coordinates equations (1), (2) and (3) are used to calculate the analytical expressions of the rotational angles (i.e. θ_1, θ_2 and θ_3) as a function of the desired x, y, and z coordinates. The derivation of the inverse kinematic equations is summarized as follows:

$$\theta_1 = atan2\left(\frac{y}{x}\right) \quad (4)$$

$$C_3 = \frac{x^2 + y^2 + z^2 - \left({L_1}^2 + {L_2}^2 + {L_3}^2\right) - 2L_1(z - L_1)}{2L_2L_3} \quad (5)$$

$$S_3 = \pm\sqrt{1 - {C_3}^2} \quad (6)$$

$$\theta_3 = atan2\left(\frac{S_3}{C_3}\right) \quad (7)$$

$$\theta_2 = atan2\left[\frac{(z - L_1)(C_1 - S_1)}{(x - y)}\right] - atan2\left[\frac{S_3L_3}{(C_3L_3 + L_2}\right] \quad (8)$$

2.2.4 Dynamics Model

The physical robotic arm was scaled down from a real excavator, so it important to know the dynamics model of the scaled manipulator. The dynamics equation is as follows:

$$\tau = M(q)\ddot{q} + C(q,\dot{q})\dot{q} + g(q) \tag{9}$$

Where $M(q)$ represents the inertial terms according to the mass distribution, 4×4 Matrix, $C(q,\dot{q})$ represents the centrifugal-force/Coriolis-force terms, 4×4 Matrix, and $g(q)$ represents the gravitational term, 4×1 Matrix, as follows.

$$\begin{bmatrix} M(1) & M(2) & M(3) & M(4) \\ M(5) & M(6) & M(7) & M(8) \\ M(9) & M(10) & M(11) & M(12) \\ M(13) & M(14) & M(15) & M(16) \end{bmatrix},$$

$$\begin{bmatrix} C(1) & C(2) & C(3) & C(4) \\ C(5) & C(6) & C(7) & C(8) \\ C(9) & C(10) & C(11) & C(12) \\ C(13) & C(14) & C(15) & C(16) \end{bmatrix},$$

$$\begin{bmatrix} G(1) \\ G(2) \\ G(3) \\ G(4) \end{bmatrix}$$

The information of the moment of inertia is taken from SolidWorks and the unit is gram·square millimeters. All details for the matrices components are available in Appendix A.

2.3 Master System

The TMSRA requires a master system to control the slave system, the physical robotic arm. In this study, 3D Systems $Touch^{TM}$ Haptic Device by Sensable Technologies was used as the master system. According to previous studies [26],[27], using haptic devices instead of conventional hydraulic joysticks improved the control efficiency and intuition. This study used the haptic device to improve the control efficiency and intuition of operators, and the haptic device has enough joints to control the slave robotic

manipulator. This haptic device was based on a serial architecture with six DOF. The workspace of the haptic device was 16 cm × 12 cm × 7 cm (W × H × D) and provided force feedback up to 3.3 N. The nominal position resolution was around 0.055 mm. The haptic device was used by grasping the stylus as a pen and moving the stylus in desired directions and speed. Figure 10 represents how each joint rotated. The described joint movements in the upper part of Figure 10 were responsible for movement in X, Y, and Z. Additionally, the joints described in the lower part of Figure 10 allowed the movement of pitch, roll, and yaw. In this study, a human operator used the joint movements of Encoder X, Encoder Y, and Encoder Z, which can be seen in the upper part of Figure 10, to change the position of the slave system. Additionally, the operator used the joint movement of Gimbal Y in the lower part of Figure 10 to open and close the end-effector of the slave system, which is either a bucket or ripper in this study. For the conventional excavator, it is not necessary to control the orientation of the attachment because the bucket is only opening and closing, so the Gimbal X and Gimbal Z were not used in this study. To control an excavator that has a rotating coupler, the Gimbal X and Gimbal Z would be necessary to control the orientation of the attachment.

Figure 10 - Movement of the Haptic Device [40]

2.4 Overall System Diagram

2.4.1 TMSRA System Diagram

The TMSRA is a bidirectional closed-loop control type and consists of two parts, namely, the master system and the slave system as seen in Figure 11. In this study, the slave system replicates the movements of an excavator's arm. The master system provides velocity information for each joint to the slave system. The slave system processes the velocity information based on the motion scaling factor to mimic the movements of the master system. A slave system, a four DoF robotic arm, is remotely controlled by a master system, 3D Systems Touch Haptic Device by Sensable Technologies. This haptic device has a pen-like stylus that a user can hold and move through the air to change the position of the physical robotic arm. The motion scaling factor is determined by the status of the buttons on the stylus of the master system. The refresh rate of the master system, the slave system, and the force/torque sensor is 1 kHz. The delay from the master system is 1000 microseconds. The delay from actuators on the slave system is 80 microseconds and the data transmission delay for Nano17 with the sampling rate of 1 kHz is 2000 microseconds. Considering all the data transmission in the system, the overall latency in the system is around 0.009 seconds. The time-delay is relatively smaller than the threshold of time-delay, 1.5 seconds. According to a study [41], the threshold of time-delay which is affected to task completion time is beyond 1.5 seconds.

Motion-scaled control is applied to the teleoperation system so that it allows the better efficiency and accuracy of work. The motion-scaled teleoperation allows for a modifiable motion ratio between the haptic device and the physical robotic arm in real-time. With the 1:1 motion scaling, the physical robotic arm travels 1cm along the x-axis if

the haptic device travels 1 cm along the x-axis. When the motion scaling is 2:1, the physical robotic arm travels two times the distance of the movement of the haptic device. Similarly, when the motion scaling is 0.5:1, the physical robotic arm travels half the distance of the movement of the haptic device.

Force feedback is applied to the TMSRA to provide the operator force feedback when the end-effector of the physical robotic arm hits an object. The ATI Nano17 sensor provides force/torque information to the haptic device. When the force/torque information is received on the haptic device, the haptic device activates its actuators to represent the force information so that the human operator can get force feedback. Once the force information is sent from the force/torque sensor, the magnitude of the force information is reduced to protect the operators. The force values from simulated construction tasks, such as excavating or demolition, are too big for the operators to hold the stylus of the haptic device, so it should be reduced.

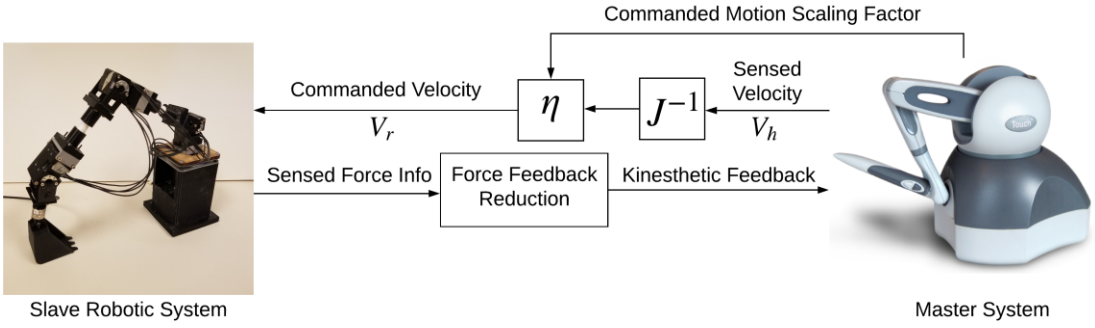

Figure 11 - Control Framework

2.4.2 Basic Information for ROS

For the TMSRA, the Robot Operating System (ROS) platform was used. ROS is an open-source software platform that contains numerous contributions from around the world. The philosophy of ROS is to make software easily for other robots by changing little in the code [42]. There are several significant terms specified in ROS, such as nodes, messages, and topics. The ROS master is the core of ROS because it provides name registration. Nodes are not able to find each other and exchange messages without the ROS master. In ROS, most functionality is divided into numerous pieces that communicate with each other using messages, where each piece is called a node. Nodes run as a separate process and communicate with each other by passing messages. Here, the message is simply a data structure, including typed fields. A node sends out a message by publishing it to a designated topic. The topic is a name that is used to identify the content of the message. A node that is concerned with a certain kind of data will subscribe to the appropriate topic. A single node may publish or subscribe to multiple topics. Also, there may be multiple concurrent publishers and subscribers for a single topic. One more significant term for ROS is a ROS package. A ROS package contains ROS nodes and a ROS-independent library, a dataset, configuration files and so on.

2.4.3 System Architecture

The teleoperation system was run on a Linux machine (Ubuntu 16.04). In this study, three ROS packages and five nodes were used to integrate the master system with the slave system. The key packages for this study were the PhantomOmni package [43] for the master system and the Dynamixel workbench package [44] for the slave system. As

described above, ROS is an open-source software platform so the packages for the haptic device and the Dynamixel motors were downloaded from open sources and modified for this study. The PhantomOmni package [43] provided the position, velocity, and acceleration information of the haptic device for each joint and the status of buttons of the stylus in real-time. Additionally, it also contained a piece of code to activate the first three actuators of the haptic device to transfer force information from the force/torque sensor to the human operator. The Dynamixel workbench package [44] was provided by ROBOTIS, the manufacturer of the Dynamixel servo motors for the physical robotic arm. This package was used to actuate motors based on the velocity information from the haptic device in this study. One more package from the open-source software platform was the package for the force/torque sensor [45]. These packages could not work for teleoperation when it solely existed without nodes to integrate each other, so four nodes were created to provide and receive required information with each other.

Figure 12 shows how packages communicate with each other. The circle represents nodes, the rectangle represents topic messages, and the names with omniEthernet are for the haptic device. The haptic device provided its velocity and button state information using the node and topic messages. The haptic device received the force information from the Nano17 sensor to represent force feedback by activating its actuators. At first, the velocity information and button status were delivered to the pose_info to make motor commands. For the motion scaling teleoperation, the velocity information was modified based on the motion scaling factor. The information on the button status was delivered to the pose_info node through the omniEthernet/button_state topic. The modified velocity information for each joint was sent to the general_velocity_control by using the

cmd_joint_vel topic message to actuate the motors. While the motor commands were processed, the netft_data provided the force information to the pose_info for a safety function. Also, netft_data provided force information to the forcefeedback node. The node modified the magnitude of the force information based on a predefined scaling factor and provided the modified force feedback value to the haptic device to represent force feedback.

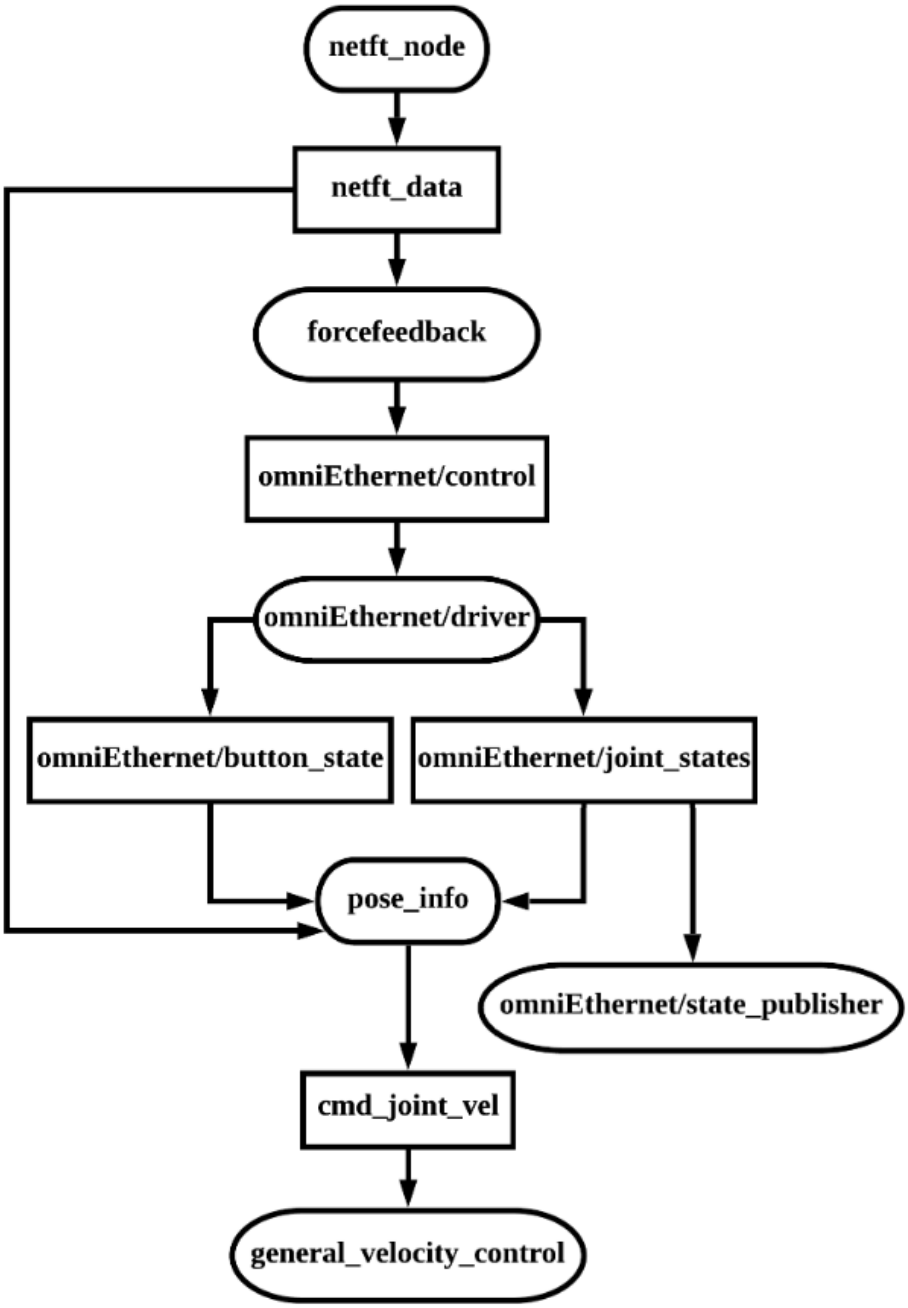

Figure 12 - Overall System Architecture in ROS

CHAPTER 3. MOTION SCALING TELEOPERATION

3.1 The Usefulness of Motion Scaling Teleoperation

As described in Chapter 2, motion scaling teleoperation allows changing the motion ratio between the master system and the slave robot system. Many tasks require manipulation in spaces too constrained or dangerous for human operation. In such cases, teleoperated robotic manipulators play an important role [46]. When we handle small scale objects in a limited space, the work cannot be done in an easy manner because we cannot see the whole target well [47]. From the above facts, it has been shown that having a teleoperated motion scaling robotic manipulator is critical to the precision and efficiency of work in various types of work environments for non-repetitive tasks. A proper interface allows for motion scaling: easy-to-perform macroscopic movements at the master's console are scaled-down in a micro-scale environment. Such systems can be used for microsurgery and lab work involving minuscule parts. In a macro-scale environment, this whole system can contribute to construction by having an end-effector for digging such as at different scaling environments [48] and it will make for less dangerous construction sites.

On construction sites, both micro-teleoperation and macro-teleoperation are required because heavy construction equipment needs careful control when performing given tasks, such as dealing with an object in a macro-scale environment. For instance, an excavator moves its arm to the workspace to perform tasks. In this case, the excavator arm would be controlled by macro-teleoperation so that the excavator arm could reach the desired position in the workspace faster than with 1:1 motion scaling. When the excavator's arm reaches the desired position, it starts to work the given missions. When performing the given tasks by manipulating the attachment of the excavator, micro-teleoperation allows

for dexterous control. By combining micro-teleoperation and macro-teleoperation for the construction equipment, it would give many advantages to the construction industry. It would be expected that motion scaling teleoperation would contribute to the construction industry in terms of better efficiency and better accuracy.

3.2 Motion Scaling Teleoperation in the TMSRA

The TMSRA was designed to change the motion scaling between the haptic device and the physical robotic arm for efficient and better control during operation. In this study, three types of motion scaling were tested: 1:1 motion scaling, 0.5:1 motion scaling, and 2:1 motion scaling. First, the 1:1 motion scaling was tested to see whether the physical robotic arm mimicked the movements of the haptic device well or not. The 1:1 motion scaling between the master system and the slave system was the baseline motion scaling for the teleoperation. The other motion scalings were modified from the 1:1 motion scaling so it was important to have a reliable 1:1 mapping movement between the master system and the slave system. Second, the 0.5:1 motion scaling was tested to see if the TMSRA could be used for micro-teleoperation. Micro-teleoperation allowed for a human operator to control the device delicately even though the operator's manipulation was rough. Third, the 2:1 motion scaling was tested to see if the TMSRA could be used for macro-teleoperation. When the TMSRA performed a task in a large simulated environment, the macro-teleoperation helped the operator to move the TMSRA faster with less movement. On construction sites, both micro-teleoperation and macro-teleoperation would be useful for efficient and better control; three types of motion scaling were tested.

3.2.1 Limitation of Position Control Algorithm for Motion Scaled Teleoperation

In this study, two control algorithms were tested for the TMSRA to implement the motion scaled teleoperation. One was a position control algorithm and the other was a velocity control algorithm. At first, the TMSRA with the 1:1 motion scaling was tested with only the position control algorithm. The haptic device provided its end-effector's absolute position information to a PC. The PC calculated the required joint displacements of the physical robotic arm for the first three joints to move to the same position as the haptic device based on inverse kinematics. After that, the PC sent the calculated joint position information to the servo motors on the physical robotic arm. The end-effector's position information of the haptic device was directly sent to the actuator for the end-effector of the physical robotic arm. Basically, the inverse kinematics determines the first three joints' displacements when the end-point position is given [37].

The position control algorithm worked well with a 1:1 motion scaling, but the position control algorithm did not work for modifiable motion scaling because the position control algorithm used the absolute position information of the haptic device to control the physical robotic arm. The physical robotic arm did not stay at the current position when the motion scaling was changed even though the haptic device remained in the same position. Let's imagine the situation that both the haptic device and the physical robotic arm are at the position of (1, 1, 1) in the Cartesian coordinates. The haptic device keeps the same position, but the motion scaling changes from 1:1 to 2:1. In this case, the physical robotic arm is supposed to keep the same position because the haptic device keeps the same position. However, the physical robotic arm actually moves to (2, 2, 2) in the Cartesian coordinates even though the haptic device does not move at all. It was because the desired

position was changed by the motion scaling factor. The desired position was multiplied by 2, which was the amount of the motion scaling factor, and the inverse kinematics was calculated based on the modified desired position. In other words, the calculated joint angles based on the inverse kinematics was for the position of (2, 2, 2), not the position of (1, 1, 1) in the Cartesian coordinates. Because of this reason, the physical robotic arm did not remain in the current position when the motion scaling changed without movement of the haptic device.

Besides this issue, the position control had one more issue for the workspace. With the position control, the workspace of the slave robot system was limited to the workspace of the master system because the position control used the absolute position information of the haptic device to control the physical robotic arm. Even though the physical robotic arm had a wider workspace than the workspace of the haptic device, the master system could not be manipulated beyond its workspace, so the slave system was not able to be controlled remotely beyond the workspace of the haptic device.

3.2.2 Velocity Control Algorithm

The velocity control algorithm resolved the described issues of the position control algorithm above. The velocity control algorithm did not use the absolute position information but used the real-time velocity information of the haptic device. Thus, changing only the motion scaling did not affect the position of the physical robotic arm. Specifically, the haptic device provided velocity information of each of its joints to the PC, and then the PC sent the velocity commands to the servo motors with the 1:1 motion scaling. The servo motors for the slave system rotated with the same velocity for the same amount

of time as each joint of the haptic device. Both the haptic device and the physical robotic arm traveled the same distance. For the 2:1 or 0.5:1 motion scaling, the PC multiplied the velocity information by 2 or 0.5 so that the physical robotic arm traveled two times or half the distance of the haptic device based on the following equation (11).

$$Distance = Velocity \times Time \tag{10}$$

The velocities of the robotic arm joints were commanded as

$$V_r = J^{-1} V_h \eta \tag{11}$$

$$J(q) = \begin{bmatrix} -S_1(L_1C_2 + L_3C_{23}) & -C_1(L_2S_2 + L_3S_{23}) & -L_3C_1S_{23} \\ C_1(L_2C_2 + L_3C_{23}) & -S_1(L_2S_2 + L_3S_{23}) & -L_3C_1S_{23} \\ 0 & L_2C_2 + L_3C_{23} & a_3C_{23} \\ 0 & S_1 & S_1 \\ 0 & -C_1 & -C_1 \\ 1 & 0 & 0 \end{bmatrix} \tag{12}$$

where J^{-1} is the inverse of the manipulator Jacobian matrix, V_h is the velocities of the haptic device joints, and η is the scaling factor between the master and slave system.

The limited-workspace issue seen with the position control algorithm was resolved by utilizing two buttons on the stylus of the haptic device (Figure 13). When pressing both the white and the grey buttons on the stylus, the slave system did not follow the movement of the master system, so that a human operator could move the stylus of the master system to a more convenient location. This is analogous to the way a computer mouse can be lifted from the surface to move the computer mouse to a more convenient location. With this function, the physical robotic arm could move beyond the workspace of the haptic device, according to the user's convenience.

Figure 13 - Buttons on the Stylus of the Haptic Device [49]

Figure 14 shows the pseudo-code of the velocity control algorithm for the TMSRA. With this algorithm, the TMSRA was able to work for modifiable motion scaled teleoperation. As described in Figure 14, the inputs for this algorithm were the button status of the haptic device and real-time velocity information of the haptic device for each joint. It determined the motion scaling factor and 'mode' at first based on the status of the buttons. The motion scaling factors were set for 1, 2, and 0.5 in this study. The 'mode' determined whether the physical robotic arm would follow the movement of the haptic device or not. The motion scaling factor was 1 when both the white and grey buttons were not pressed. The motion scaling factor was 2 with pressed the grey button and 0.5 with pressed the white button. For these cases, the 'mode' was 0, and it allowed for the physical robotic arm to mimic the master's movements based on the motion scaling factors. The only exception was when both the white and grey buttons were pressed. In this case, the 'mode' was 1, and the physical robotic arm never moved even though the human operator manipulated

the haptic device. The real-time velocity information of the haptic device was multiplied by 0. The calculated values were the velocity commands to the servo motors on the physical robotic arm. The velocity commands to the motors were 0 and the physical robotic arm did not move when the ‘mode’ was 1. For the ‘mode’ of 0, the determined motion scaling factor was multiplied by the real-time velocity information of the haptic device for each joint. For example, if the human operator kept the white button pressed while manipulating the stylus, the motion scaling factor changed to 0.5 and the physical robotic arm traveled only half of the travel distance of the stylus. Then, if the human operator released the white button, the motion scaling would change back to 1:1. In this way, the human operator could utilize the three types of motion scaling factor to make their work easier and more efficient.

Algorithm 1 Pseudo Code for Modifiable Motion Scaled Teleoperation

```
0: input 1 ← white button status of the haptic device
0: input 2 ← grey button status of the haptic device
0: input 3 ← a = real time velocity information of haptic device for joint 1
0: input 4 ← b = real time velocity information of haptic device for joint 2
0: input 5 ← c = real time velocity information of haptic device for joint 3
0: input 6 ← d = real time velocity information of haptic device for joint 4
1: if white button is not pressed && grey button is not pressed then
2:    motion = 1;
3:    mode = 0;
4: else if white button is not pressed && grey button is pressed then
5:    motion = 2;
6:    mode = 0;
7: else if white button is pressed && grey button is not pressed then
8:    motion = 0.5;
9:    mode = 0;
10: else if white button is pressed && grey button is pressed then
11:   mode = 1;
12: end if
13:
14: if mode = 0 then
15:   vel. of motor 1 = a x motion;
16:   vel. of motor 2 = b x motion;
17:   vel. of motor 3 = c x motion;
18:   vel. of motor 4 = d x motion;
19: else
20:   vel. of motor 1 = a x 0;
21:   vel. of motor 2 = b x 0;
22:   vel. of motor 3 = c x 0;
23:   vel. of motor 4 = d x 0;
24: end if=0
```

Figure 14 - Pseudo Code for Modifiable Motion Scaled Teleoperation

3.3 Experimental Setting for Motion Scaling Teleoperation

3.3.1 Hypothesis

The experiment for motion scaling teleoperation was performed to see the effect of motion scaling teleoperation. The major hypothesis for this experiment was that task completion time would be reduced when utilizing motion-scaled control. Additionally, motion scaling teleoperation would allow for delicate control so that the task completion time for tasks that required delicate control would be more reduced.

3.3.2 Study Protocol for Motion Scaling Teleoperation

The experiment required subjects to interact with the haptic device. 10 human subjects were given the task to manipulate the stylus of the haptic device to make the physical robotic arm move a small piece of plastic to Pos 1, Pos 2, and Pos 3 separately as seen in Figure 15. Initially, subjects were provided 15 minutes to familiarize themselves with the system so that the task time did not improve over trials.

In the first round of the test, the tasks were performed with the three target positions, Pos 1, Pos 2, and Pos 3, having a surface area of 2.5 cm^2, but without the motion scaling. The subjects performed the task 10 times for each position. During this experiment, the time that was required to fit the small piece of plastic into Pos 1, Pos 2, and Pos 3, respectively, was recorded. In the second round, the human subject was allowed to use the motion scaling to control the physical robotic arm for the same task as the first round of the test with the position surface area of 2.5 cm^2. In the third round, the same tasks were performed with the three target positions having a surface area of 3.0 cm^2, but without the motion scaling. In the fourth round, the human subject allowed to use the motion scaling

for the same tasks with a position surface area of 3.0 cm^2. At the end of the four rounds, the human subject had performed 120 trials.

Figure 15 shows the experimental setup to demonstrate motion scaling teleoperation of the TMSRA. For the initial configuration of the test, the physical robotic arm was placed on the space marked "ROBOT", while the bucket was placed on "Bucket Position" in Figure 15. A 2 cm^3 cube of plastic was placed on "Piece" at the beginning of the test. There were three target positions, each progressively farther from the robot base. Pos 1 was placed on the same line as the "Piece" on the board, and it was the closest position for the physical robotic arm to move the small piece of plastic to. However, because the robotic arm moved in an arc, not in a straight line, it was not possible for the physical robotic arm to just move along the line to put the small piece of plastic into Pos 1. Pos 2 was not on the same line as the Piece, and this target position was determined to have a more difficult position to get than the Pos 1. Lastly, Pos 3 was the farthest target position, and the physical robotic arm needed to be almost fully extended to move the small piece of the plastic to Pos 3.

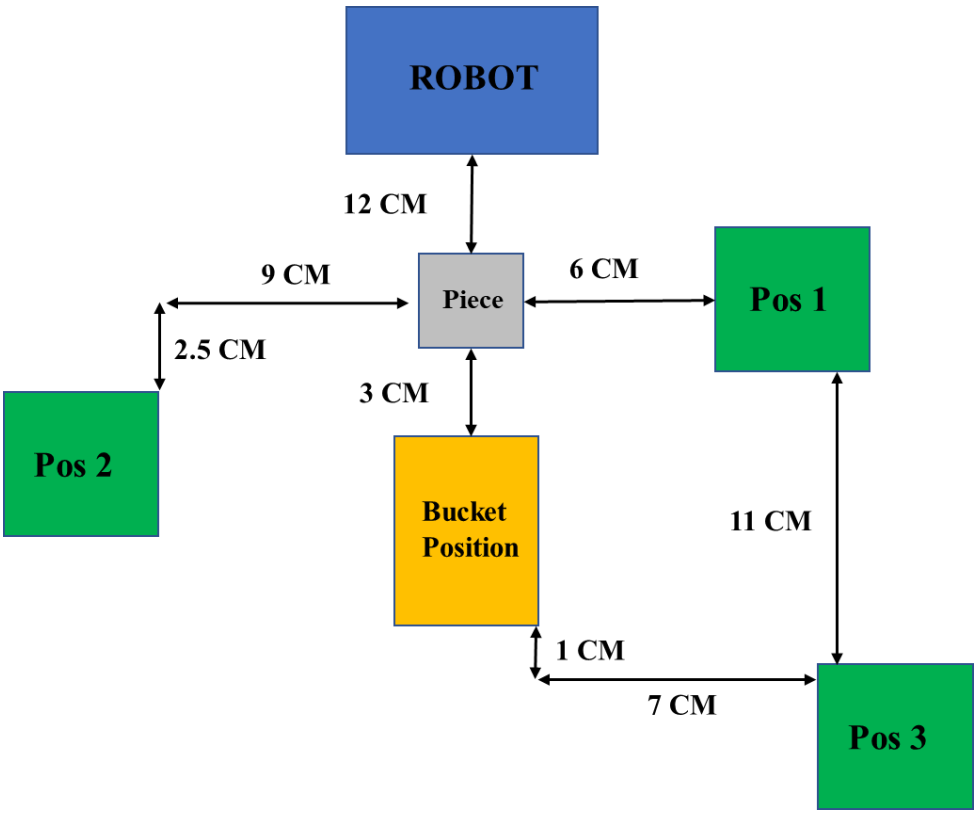

Figure 15 - Experimental Setting for Motion Scaling Teleoperation

3.3.3 Data Analyzing Method

As mentioned above, the time that was required to fit the small piece of plastic into Pos 1, Pos 2, and Pos 3, respectively, was recorded. To see the effect of the motion scaling teleoperation, the recorded task completion time was compared between the first round of test and the second round of the testTo see the effect of the motion scaling teleoperation, the recorded task completion time was compared between the first round of test and the second round of the test and between the third round of test and the fourth round of the test. The recorded task completion time between The recorded task completion time between the first two rounds of the test and the last two rounds of the test was compared to see the

effect of motion scaling teleoperation for was compared to see the effect of motion scaling teleoperation for precise control. control. The difference between the first two rounds of the test and the last two rounds of the test was the surface area of target positions: 2.5 cm^2 and 3 cm^2. The diagonal length of the small piece of plastic was 2.83 cm so having two different surface areas demonstrated the utility of motion scaling for precise control. The small piece of plastic should, in theory, be difficult to fit into the surface with the area of 2.5 cm^2 because the diagonal length was larger than a side of the surface. The side of the small piece of plastic should be almost parallel to the side of the surface for the small piece of plastic to be fitted into the surface. On the other hand, the small piece of the plastic should be easier theoretically to fit into the surface with the area of 3 cm^2 no matter what the configuration of the small piece of the plastic was.

Another difference between tests one and two and between tests three and four was the existence of the motion scaling. Comparing those cases should provide enough data to determine if the motion scaling improves the efficiency of work.

3.3.4 Expected Experimental Results

The task completion time was expected to be reduced when using the motion scaling teleoperation. The effect of the motion scaling teleoperation was expected to be observed by comparing the experimental results between tests one and two and between tests three and four. Also, the bigger effect of motion scaling teleoperation was expected for the tasks that required delicate control. This would be observed by comparing the reduction rate of between the tests one and two and between tests three and four for each position

3.4 Experimental Result of Motion Scaling Teleoperation with the TMSRA

Figures 16-27 shows the average task time data with error bars for the maximum task time and the minimum task time or standard deviation for position 1, position 2, and position 3 with the surface area of 3.0 cm^2 and surface area of 2.5 cm^2 over 10 trials. The error bars were acquired by subtracting the average task time from the maximum and minimum task time from 10 subjects for each trial. These time data graphs showed that the task time was not decreasing over trials because enough practice was given to the subjects before the actual experiments to control the other factor that could affect the data.

The data in figure 16 shows the average task time for position 1 and the surface area of 3.0 cm^2 among 10 subjects over trials without and with motion scaling. The ranges of the average task time without and with motion scaling are between 26.30 seconds and 31.40 seconds and between 13.52 seconds and 20.50, respectively. The maximum task time and the minimum task time without motion scaling were 77.78 seconds and 3.99 seconds, respectively. The maximum task time and the minimum task time with motion scaling were 43.26 seconds and 3.78 seconds, respectively.

Figure 17 shows the average task completion time with standard deviation for position 1 and the surface area of 3.0 cm^2. The average standard deviation over 10 trials was 12.62 seconds without motion scaling and 8.60 seconds with motion scaling.

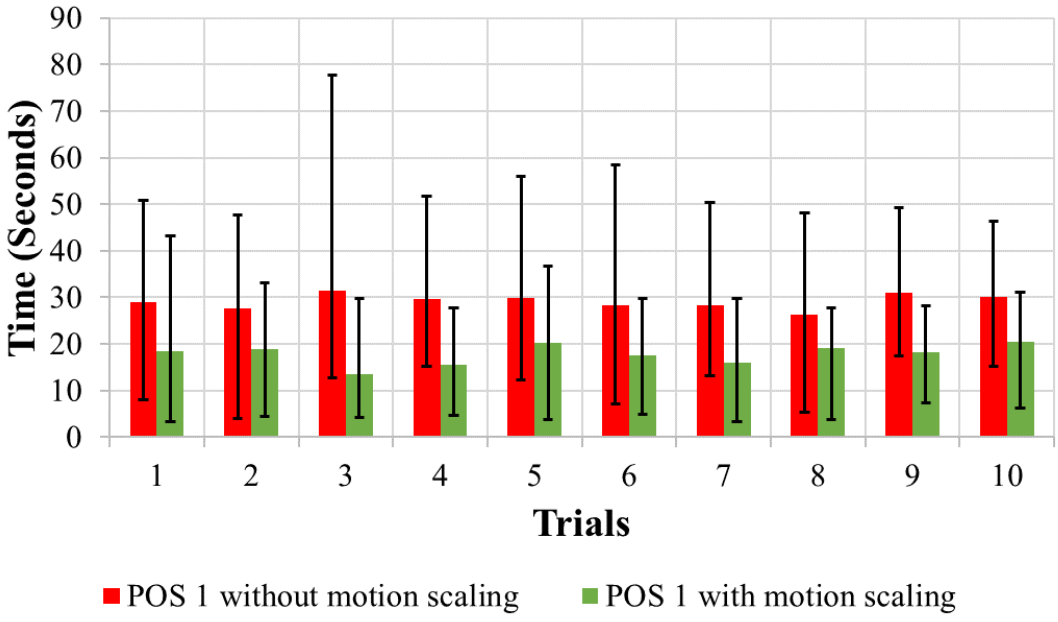

Figure 16 - Average Task Completion Time for Position 1 and Surface Area of 3.0 cm^2 over trials

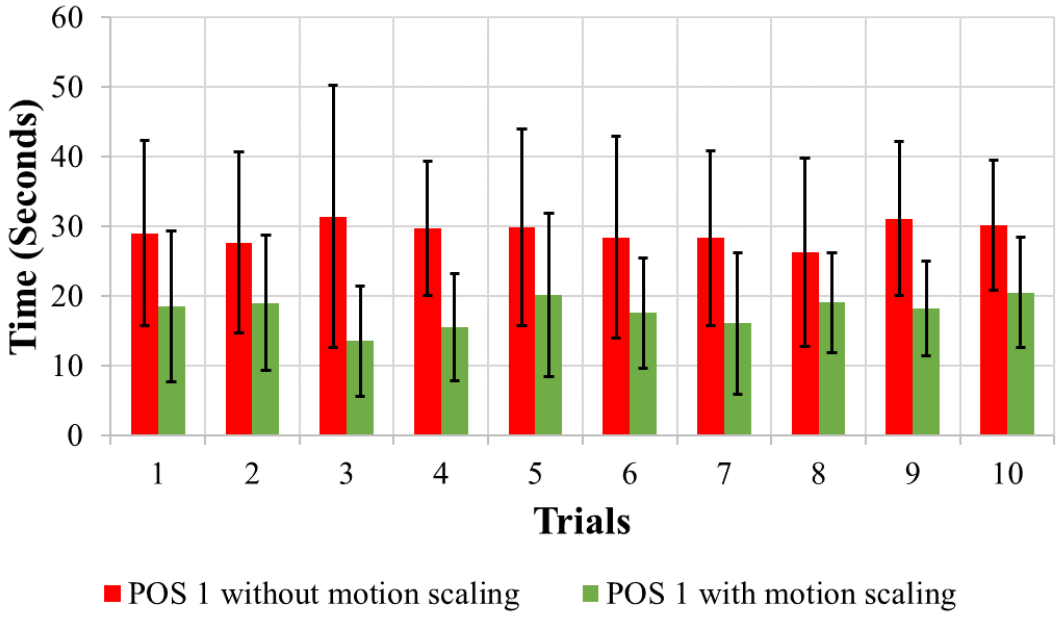

Figure 17 - Average Task Completion Time with Standard Deviation for Position 1 and Surface Area of 3.0 cm^2 over trials

Figure 18 shows the average task time for position 2 and the surface area of 3.0 cm^2 among 10 subjects over trials without and with motion scaling. The ranges of the average task time without and with motion scaling are between 38.23 seconds and 47.61 seconds and between 24.12 seconds and 29.50 seconds, respectively. The maximum task time and the minimum task time without motion scaling were 78.04 seconds and 15.93 seconds, respectively. The maximum task time and the minimum task time with motion scaling were 60.45 seconds and 8.45 seconds, respectively.

Figure 19 shows the average task completion time with standard deviation for position 2 and the surface area of 3.0 cm^2. The average standard deviation over 10 trials was 12.47 seconds without motion scaling and 9.40 seconds with motion scaling.

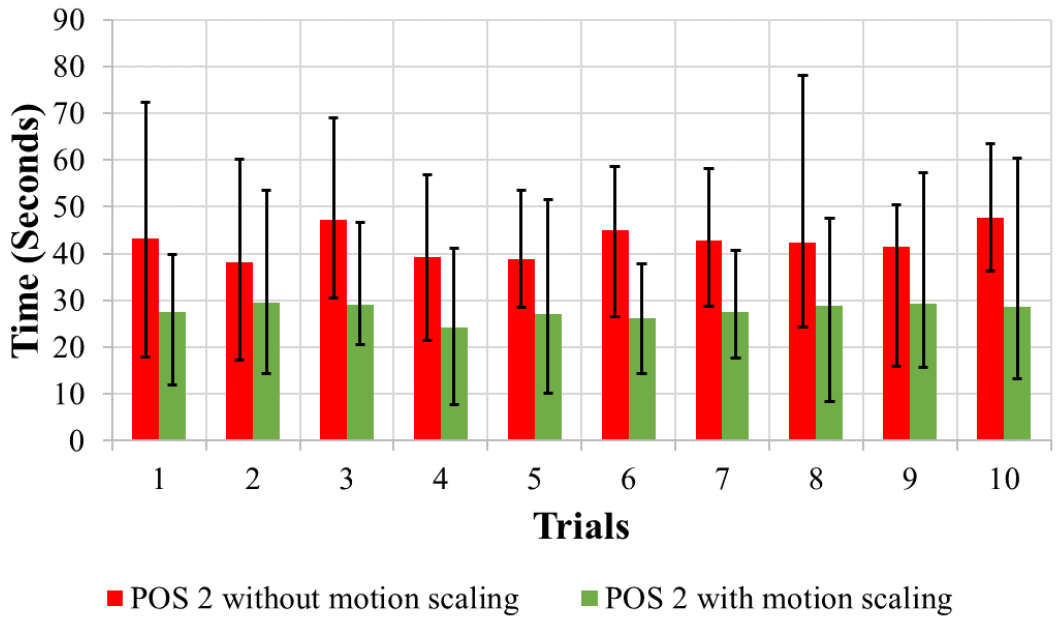

Figure 18 - Average Task Completion Time for Position 2 and Surface Area of 3.0 cm^2 over trials

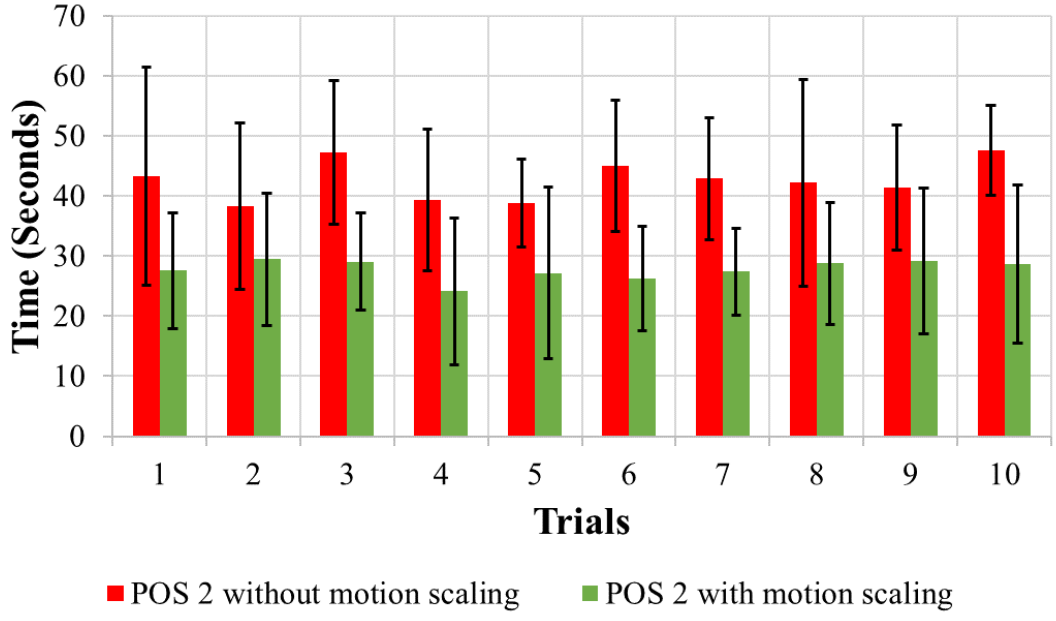

Figure 19 - Average Task Completion Time with Standard Deviation for Position 2 and Surface Area of 3.0 cm^2 over trials

Figure 20 shows the average task time for position 3 and the surface area of 3.0 cm^2 among 10 subjects over trials without and with motion scaling. The ranges of the average task time without and with motion scaling are between 39.31 seconds and 58.29 seconds and between 27.71 seconds and 38.95 seconds, respectively. The maximum task time and the minimum task time without motion scaling were 113.71 seconds and 13.23 seconds, respectively. The maximum task time and the minimum task time with motion scaling were 74.50 seconds and 5.28 seconds, respectively.

Figure 21 shows the average task completion time with standard deviation for position 3 and the surface area of 3.0 cm^2. The average standard deviation over 10 trials was 15.37 seconds without motion scaling and 11.34 seconds with motion scaling.

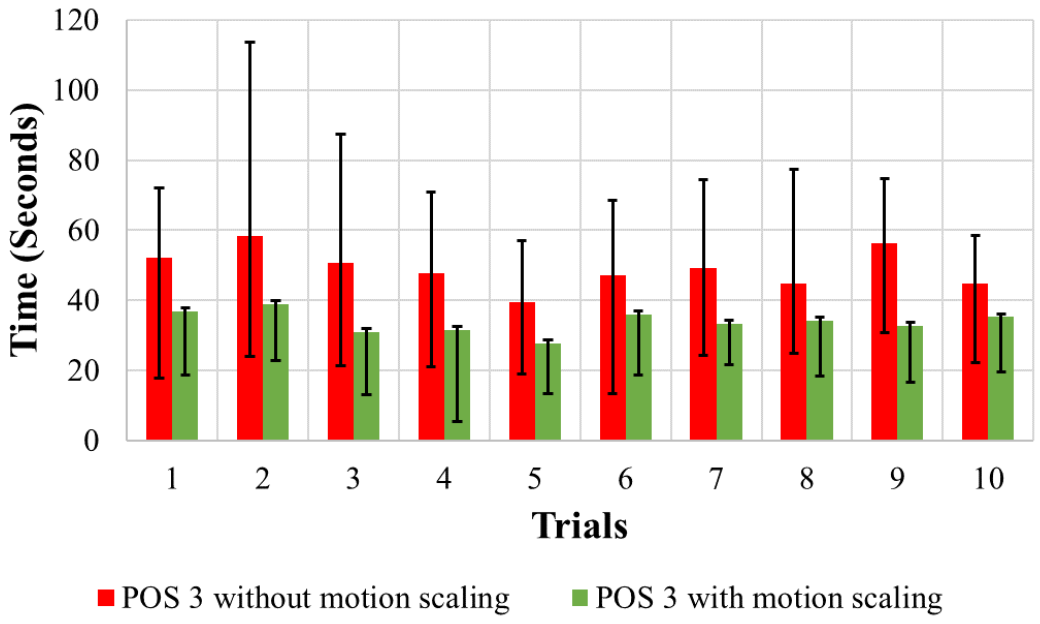

Figure 20 - Average Task Completion Time for Position 3 and Surface Area of 3.0 cm^2 over trials

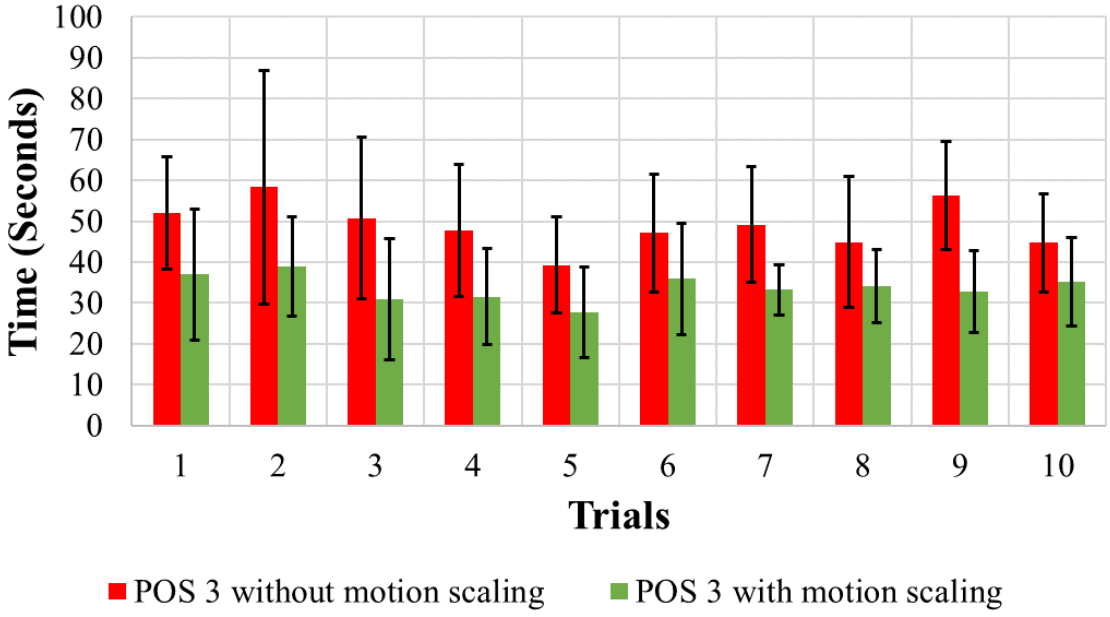

Figure 21 - Average Task Completion Time with Standard Deviation for Position 3 and Surface Area of 3.0 cm^2 over trials

Figure 22 shows the average task time for position 1 and the surface area of 2.5 cm^2 among 10 subjects over trials without and with motion scaling. The ranges of the average task time without and with motion scaling are between 54.59 seconds and 83.40 seconds and between 28.81 seconds and 37.38 seconds, respectively. The maximum task time and the minimum task time without motion scaling were 180 seconds and 12.28 seconds, respectively. The maximum task time and the minimum task time with motion scaling were 88.10 seconds and 3.20 seconds, respectively.

Figure 23 shows the average task completion time with standard deviation for position 1 and the surface area of 2.5 cm^2. The average standard deviation over 10 trials was 34.40 seconds without motion scaling and 16.37 seconds with motion scaling.

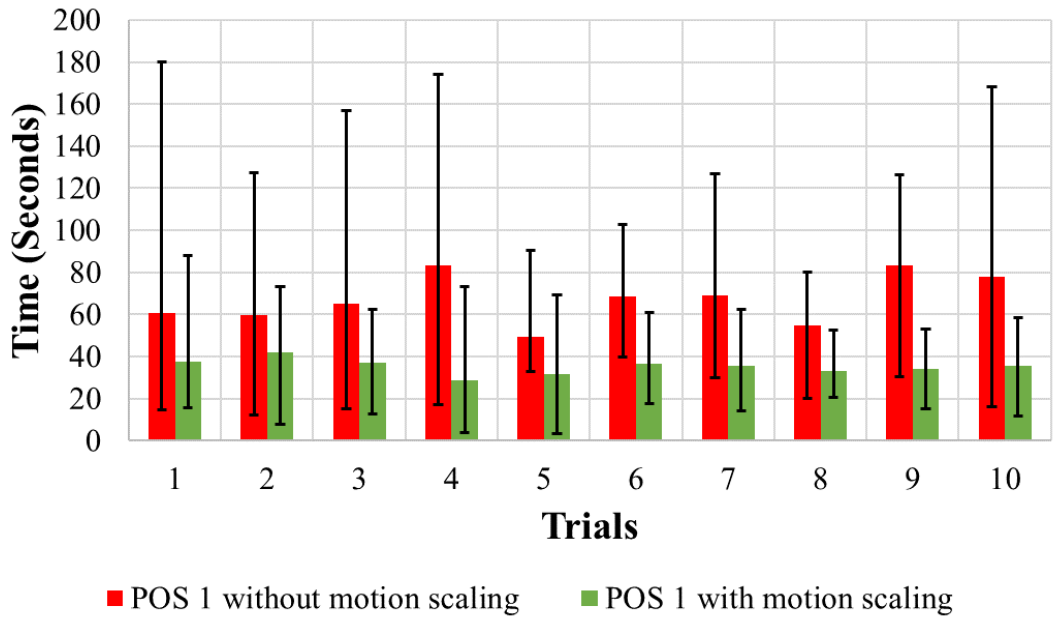

Figure 22 - Average Task Completion Time for Position 1 and Surface Area of 2.5 cm^2 over trials

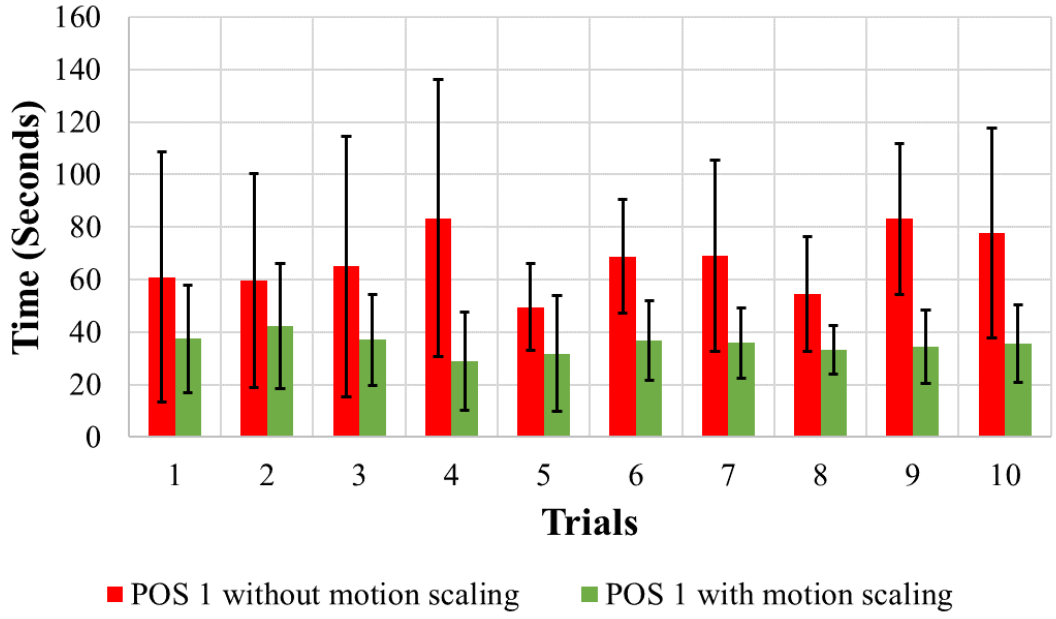

Figure 23 - Average Task Completion Time with Standard Deviation for Position 1 and Surface Area of 2.5 cm^2 over trials

Figure 24 shows the average task time for position 2 and the surface area of 2.5 cm^2 among 10 subjects over trials without and with motion scaling. The ranges of the average task time without and with motion scaling are between 52.66 seconds and 104.93 seconds and between 36.08 seconds and 50.74 seconds, respectively. The maximum task time and the minimum task time without motion scaling were 225.21 seconds and 21.43 seconds, respectively. The maximum task time and the minimum task time with motion scaling were 84.10 seconds and 9.43 seconds, respectively.

Figure 25 shows the average task completion time with standard deviation for position 2 and the surface area of 2.5 cm^2. The average standard deviation over 10 trials was 43.07 seconds without motion scaling and 15.95 seconds with motion scaling.

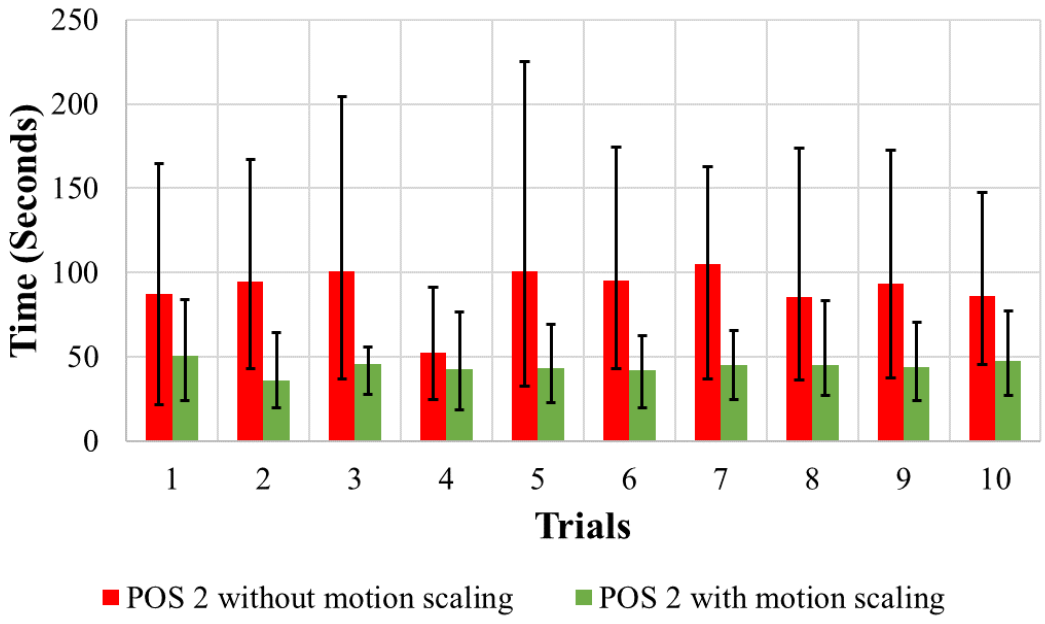

Figure 24 - Average Task Completion Time for Position 2 and Surface Area of 2.5 cm^2 over trials

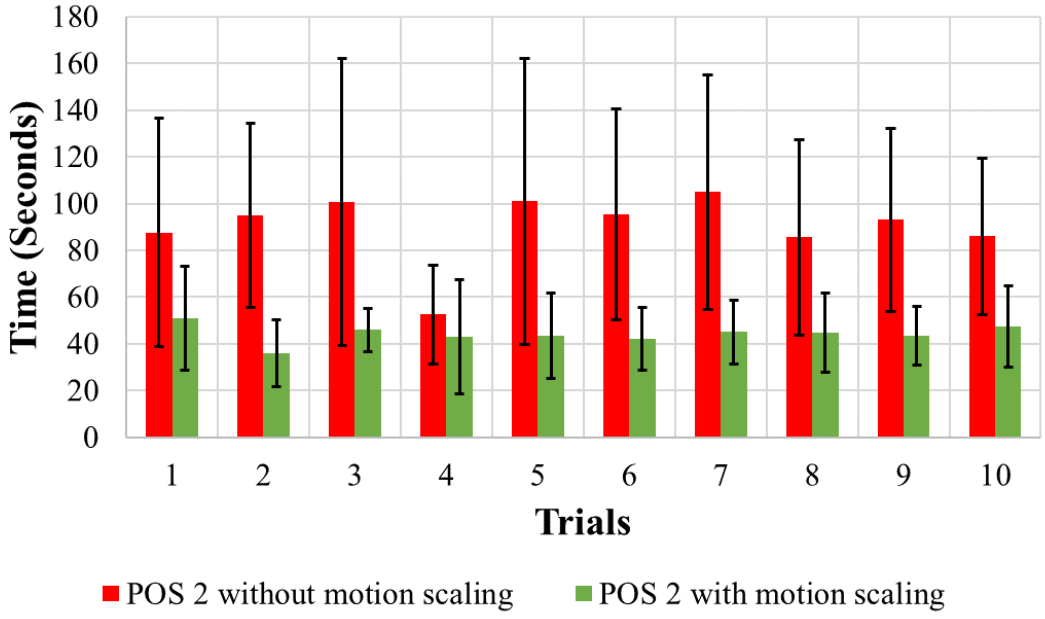

Figure 25 - Average Task Completion Time with Standard Deviation for Position 2 and Surface Area of 2.5 cm^2 over trials

Figure 26 shows the average task time for position 3 and the surface area of 2.5 cm^2 among 10 subjects over trials without and with motion scaling. The ranges of the average task time without and with motion scaling are between 83.68 seconds and 127.70 seconds and between 42.92 seconds and 58.85 seconds, respectively. The maximum task time and the minimum task time without motion scaling were 264.17 seconds and 24.86 seconds, respectively. The maximum task time and the minimum task time with motion scaling were 120.13 seconds and 13.90 seconds, respectively.

Figure 27 shows the average task completion time with standard deviation for position 3 and the surface area of 2.5 cm^2. The average standard deviation over 10 trials was 49.03 seconds without motion scaling and 20.12 seconds with motion scaling.

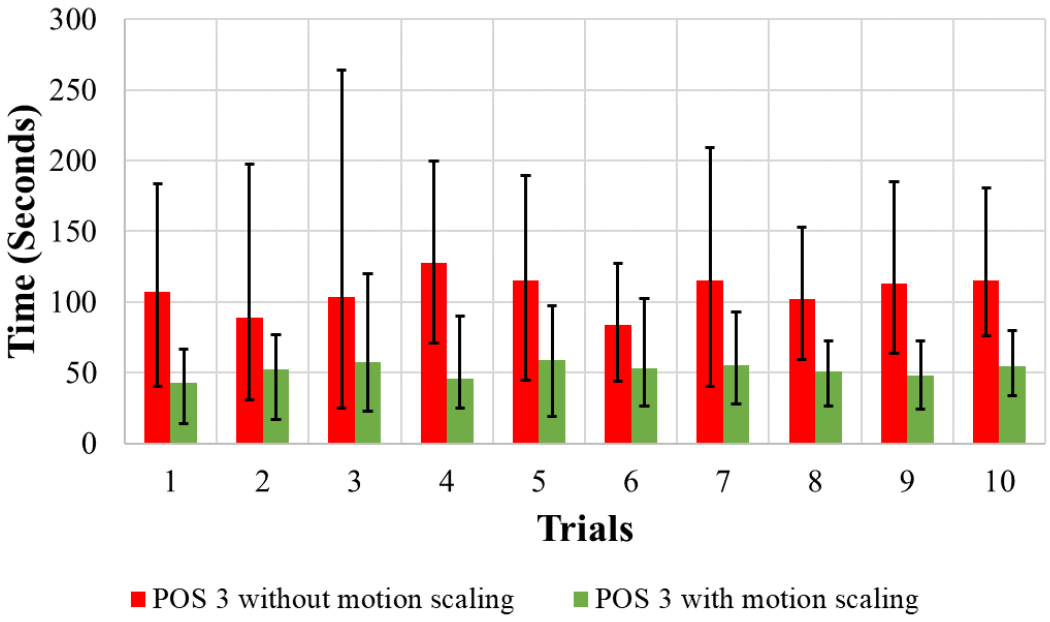

Figure 26 - Average Task Completion Time for Position 3 and Surface Area of 2.5 cm^2 over trials

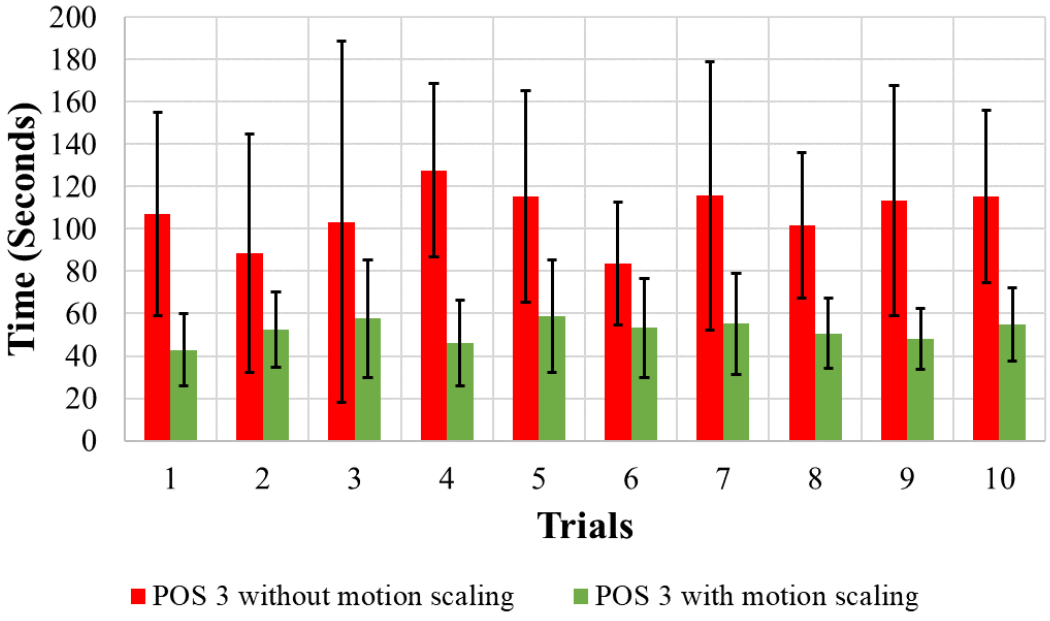

Figure 27 - Average Task Completion Time with Standard Deviation for Position 3 and Surface Area of 2.5 cm^2 over trials

Below, Figure 28 shows the average completion time among 10 subjects for the third and fourth rounds of the test. The average completion time for the third round of tests was 29.19, 42.61 and 49.01 seconds, respectively. The average completion time for the fourth round of the test was 17.80, 27.77, and 33.71 seconds, respectively. Figure 29 shows the average completion time for the first and second rounds of the test. The average completion time for the first round of tests was 67.15, 90.20, and 107.15 seconds, respectively. The average completion time for the second round of tests was 35.29, 44.21 and 51.97 seconds, respectively. The difference between the black dots and the golden dots for each position showed the effect of the motion scaling. The percentage decrease in completion time for the task with the larger area was 39.71%, 35.02%, and 31.41% for position 1, position 2, and position 3, respectively. The percentage decrease in task time for the task with the smaller area was 44.80%, 44.66%, and 47.76% for position 1, position 2, and position 3, respectively.

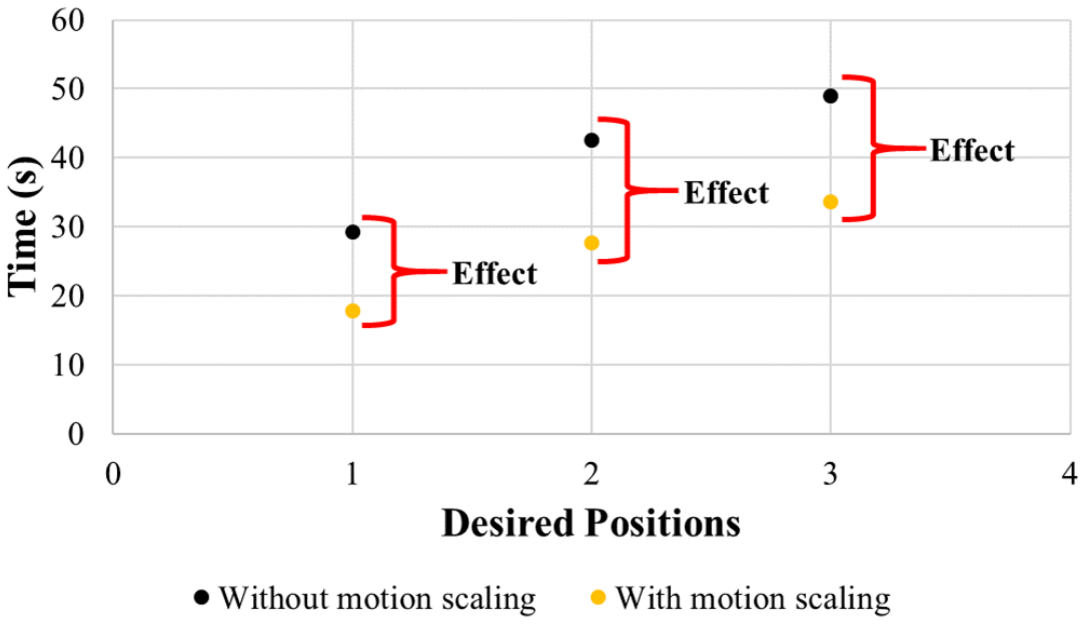

Figure 28 - Average Task Completion Time with Surface Area of 3.0 cm^2

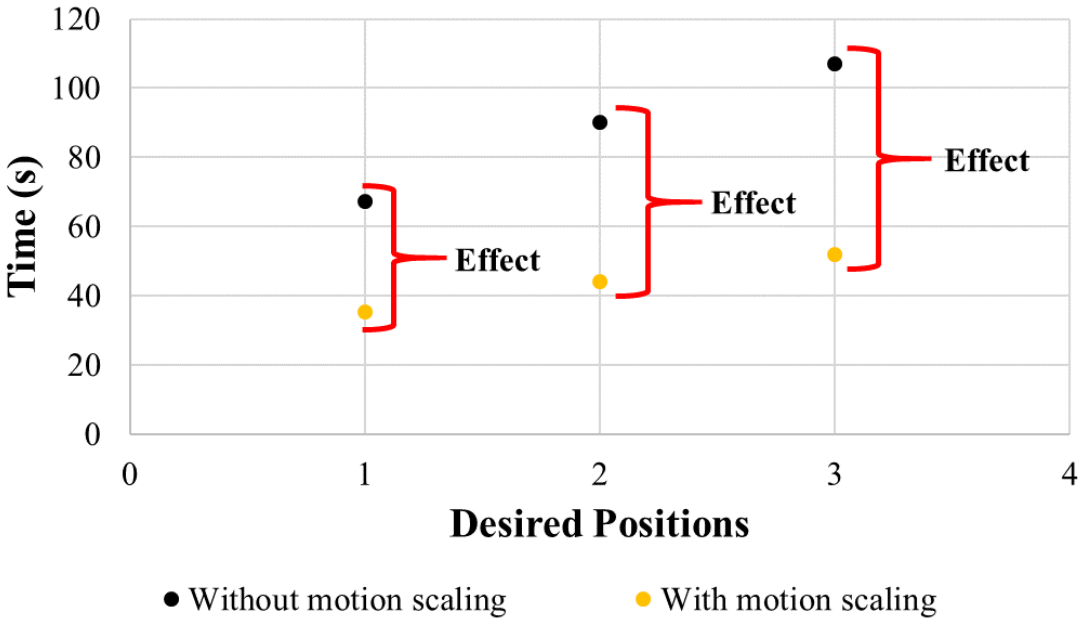

Figure 29 - Average Task Completion Time with Surface Area of 2.5 cm^2

CHAPTER 4. **FORCE FEEDBACK**

4.1 The Usefulness of Force Feedback

As the number of using teleoperation increases in remote and hazardous environments and the field of surgical robotics, researchers keep trying to improve the human capabilities for the remote manipulation of equipment. One of the efforts is providing the necessary information to a human operator for the interaction with the remote location. In this context, a haptic interface helps a human operator to interact with the remote environment through tactile feedback. Haptics could be defined as the field of experiencing and creating touch sensations in human operating mechanical devices [50]. Haptic teleoperation provides telepresence by allowing a human operator to control a slave robot remotely through a master device and to perceive the remote environment [51]. The empirical evaluations that have followed show that providing force feedback in teleoperation improves task completion times [52] and task accuracy [53], [54].

Haptic interaction between a human operation and a robotic arm through force feedback could decrease many accidents on construction sites if implemented on construction equipment. As discussed in Chapter 2, excavating near buried facilities is the biggest part of the root cause of construction accidents. By applying force feedback to the construction heavy equipment, it would be expected to prevent many accidents relating to excavation work in advance. If a human operator of the construction equipment hit buried facilities by mistake during digging or demolition tasks, the buried facilities under the construction site would be damaged. According to an article [55], the buried facilities include sanitary and storm sewers, underdrain, water, natural gas, oil, telephone, fiber optic, cable television, traffic signal, electric power, process piping, steam lines and more. If the

excavation work damages the underground facilities, it would result in a range from an inconvenience to a catastrophe. Damaged a telephone conduit and water or sewer main would bring a lot of inconveniences and breaking a pressurized gas main could fuel an explosion and fire large enough to destroy an entire neighborhood [56]. Force feedback could play an important role in preventing underground utilities from being damaged by excavation and demolition tasks. When teleoperated construction equipment with force feedback makes contact with the buried facilities, human operators could recognize the impact right away and they could take proper action not to damage the facilities. Because of this reason, force feedback would be very useful on construction sites.

4.2 Force Feedback with the TMSRA

The TMSRA was designed to transmit force information from the end-effector of the physical robotic arm to the haptic device. Due to the force feedback, human operators could realize what happened on the end-effector of the physical robotic arm. Thus, the human operator could take the proper action to finish the work successfully without incident.

Additionally, the safety function protected the facilities even though the operators did not take proper action not to damage the facilities. The safety function was actuated when the force value of the end-effector of the robotic arm was above the threshold value. It made the entire system immediately stop and rotated the distal actuator in the reverse direction a little bit not to apply external force anymore on the pipe.

In this study, the magnitude of force feedback was decreased intentionally from the force information of Nano17 because the applied force on the pipe was too large. When the same magnitude of the applied force was transmitted to the operators, they could not

hold the stylus of the haptic device well. The force information from the Nano17 was divided by a reduction ratio of 30 to decrease the magnitude of force feedback. Then, the modified value was sent to the haptic device to represent force feedback to the operators.

In this study, the marked force direction to the end-effector of the physical robotic arm in Figure 30 was more important than the other direction of the force. The reason was that the fictive buried objects of the simulated experimental setting were placed perpendicular to the end-effector in this study. When the end-effector touched a fictive pipe, the force value for the marked direction was sharply increased.

According to a study, haptic feedback latency below 30-50 milliseconds is generally perceived as instantaneous [57]. As introduced in Section 2.4.1, the total time delay in the system was around 9 milliseconds. The latency in the system was enough to facilitate haptic transparency so the system did not impede the flow of the work.

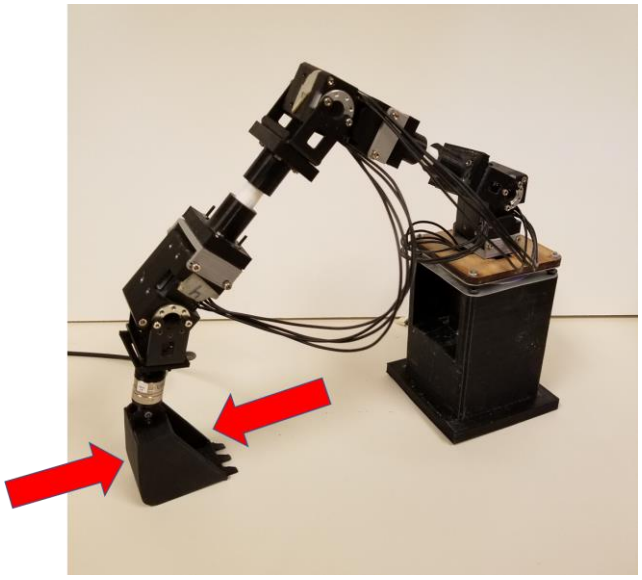

Figure 30 - Physical Robotic Arm with Force Direction

Figure 31 shows pseudo-code for the safety function. Though the Nano17 transmitted the force information for all axes, the only force information for the z-axis was referred for the safety function. When the absolute force value of the force information for the z-axis was above ‘value’, the distal joint for the end-effector rotated in the reverse direction not to exceed the ‘value’. As a result, the end-effector of the robotic arm could not apply excessive force on the pipes. The refresh rate between the Nano17 and the motors was 1 kHz so that the distal joint rotated in the reverse direction with very low response time.

Algorithm 2 Pseudo Code for Safety Function

```
0: input 1 ← force.x = force information for the x-axis
0: input 2 ← force.y = force information for the y-axis
0: input 3 ← force.z = force information for the z-axis
1: if force.z > value then
2:    set = 1;
3: else if force.z < -value then
4:    set = 2;
5: end if
6:
7: if set = 1 then
8:    vel. of motor 1 = 0;
9:    vel. of motor 2 = 0;
10:   vel. of motor 3 = 0;
11:   vel. of motor 4 = -0.5;
12: else
13:   vel. of motor 1 = 0;
14:   vel. of motor 2 = 0;
15:   vel. of motor 3 = 0;
16:   vel. of motor 4 = 0.5
17: end if=0
```

Figure 31 - Pseudo Code for the Safety Function

4.3 Experimental Setting for the TMSRA with Force Feedback

4.3.1 Hypothesis

The major hypothesis for the experiment of force feedback was that the maximum force value applied to an object would be reduced when force feedback was available. The operators of the TMSRA could recognize the impact well due to force feedback. Additionally, the maximum force value would be reduced more when both force feedback and a virtual safety function were available. The virtual safety function help prevent excessive force application by the slave device.

4.3.2 Study Protocol for the TMSRA with Force Feedback

The subjects manipulated the haptic device to dig perlite from a box and move it to another box for four different tests to see the effect of force feedback. The first test was performing the digging task without force feedback and buried plastic bars five times. Except for the first test, the holes on the side of the box as seen in Figure 34 were used to fix three plastic bars. The plastic bars under perlite to act like unforeseen obstacles for the operator. The second test was performing the digging test with three buried plastic bars and without haptic feedback five times. The third test was performing the digging test with three buried plastic bars and haptic feedback five times. The last test was performing the digging test with three buried plastic bars, haptic feedback, and safety function five times. During this experiment, the force value at the end-effector of the robotic arm was recorded. The next experiment was the demolition task with a ripper, a common end-effector used on construction equipment. Similarly, the force value at the end-effector of the robotic arm was recorded. For the demolition experiment, four different tests were conducted, similar

to the excavating experiment. However, the subjects manipulated the haptic device to crush moist sand (Figure 33). For the demolition trial, the subjects tried to crush the moist sand five times for each test.

Figure 32 - Perlite with Plastic Bars

Figure 33 - Sand with Plastic Bars

Figure 34 - Holes for Plastic Bars

4.3.3 Data Analysing Method

During the simulated excavating and demolition tests, the force information of the end-effector was recorded. Then, the maximum force value of each trial was taken and the average maximum force values were calculated for the three different tests of the excavating and demolition tasks, respectively. By plotting graphs with the calculated average maximum force values, the effects of force feedback and safety function were observed. Also, error bars in graphs showed how different the maximum values were between tests. The error bars were acquired by subtracting the average maximum force value from the maximum force value for each trial.

4.3.4 Expected Experimental Results

The maximum force values for the simulated excavating and demolition tasks without force feedback and safety function were expected to be larger than the maximum force values from the tests with force feedback and safety function. Additionally, the maximum force values from the test with only force feedback were expected to be larger than the maximum force values from the test with both force feedback and safety function. Even though force feedback was expected to help the operators recognize the impact well, it was not expected to improve the reaction time of the operators. The safety function did not improve the reaction time but it was designed not to allow excessive force on objects.

4.4 Experimental Result of the TMSRA with Force Feedback

Figure 35 shows the average maximum force values for each trial during the excavating experiments among 10 subjects. The average value was 59.01 N without the force feedback, 32.24 N with the force feedback, and 13.18 N with the force feedback and a safety function. The maximum and minimum force value without force feedback among 10 subjects was 74.07 N and 37.36 N, respectively. The maximum and minimum force value with force feedback among 10 subjects was 51.69 N and 15.76 N, respectively. The maximum and minimum force value with both force feedback and safety function was 21.71 N and 3.67 N, respectively. The average maximum force value decreased by 45.45% using the force feedback, and 77.67% using the force feedback and a safety function together.

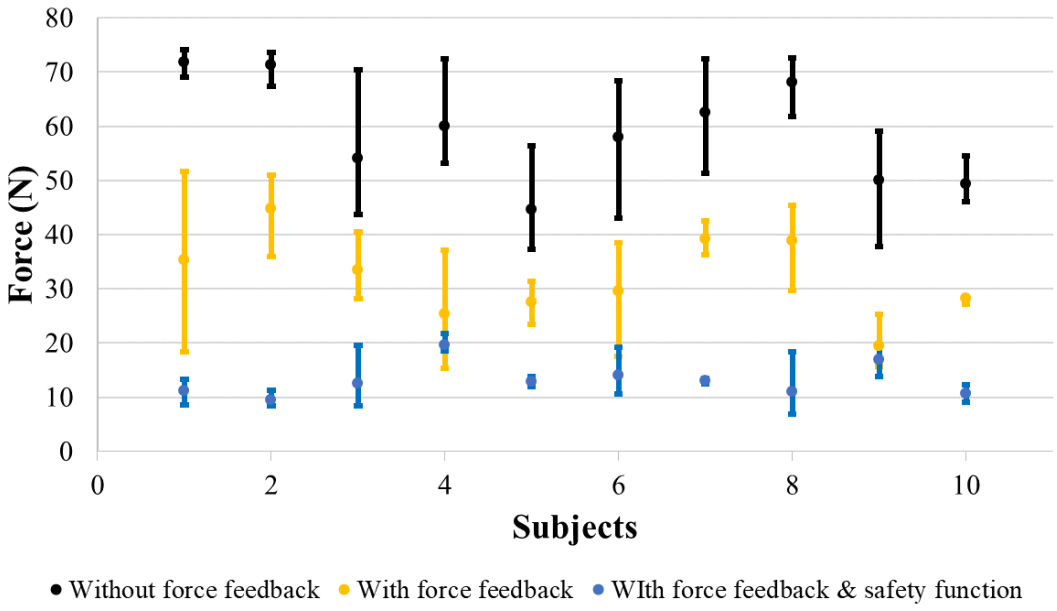

Figure 35 - Average Maximum Force for Excavating Task

Figure 36 shows the average maximum force values for each trial during the demolition test among 10 subjects. The average value was 53.64 N without the force feedback, 30.95 N with the force feedback, and 12.68 N with the force feedback and a safety function. The maximum and minimum force value without force feedback among 10 subjects was 72.91 N and 32.22 N, respectively. The maximum and minimum force value with force feedback among 10 subjects was 59.66 N and 7.84 N, respectively. The maximum and minimum force value with both force feedback and safety function was 20.52 N and 6.91 N, respectively. The average maximum force value decreased by 42.46% using the force feedback, and 76.36% using the force feedback and a safety function together.

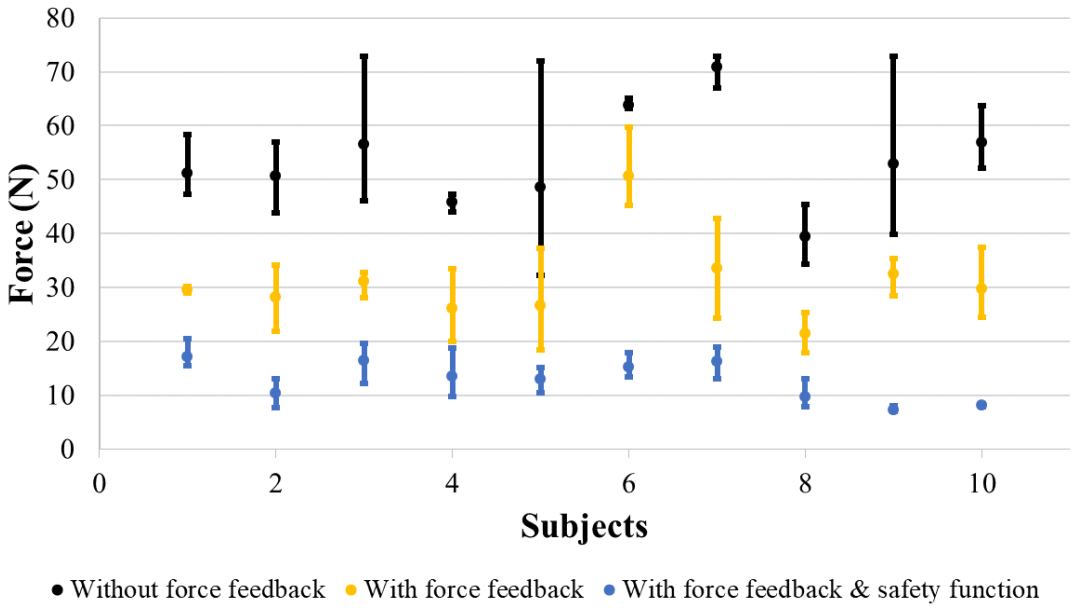

Figure 36 - Average Maximum Force for Demolition Task

CHAPTER 5. DISCUSSION AND CONCLUSION

5.1 Discussion

5.1.1 Motion Scaling Teleoperation

The experimental results in section 3.4 showed the effect of motion scaling. The completion time from the experiments differed between subjects because of individual differences. Some of the subjects got used to manipulating the master system very quickly and their completion time for motion scaling experiments was much faster than others.

Even though some of the subjects finished the given tasks very quickly and others completed the tasks slower, the experimental results showed that adopting motion scaling to the teleoperated robotic arm reduced completion times by at least 31.41% and as much as 47.76%. During the experiments, most subjects were also sometimes lucky so that they could make it easier for one or two trials out of ten trials. The average task time for position 2 without motion scaling in Figure 24 was very low because one of the subjects recorded 24.36 seconds for the task. It was much faster than the average task time for position 2 without motion scaling, 90.2008 seconds. He was very lucky for the fourth trial that the piece of plastic slid into the small surface area very quickly without delicate control.

The completion times decreased for all cases when motion scaling teleoperation was used. The motion scaling teleoperation caused a bigger decrease in the completion time for the task with the surface with the area of 2.5 cm^2 than the task with the surface with the area of 3.0 cm^2. The reason was that more delicate control was required for the task with the smaller surface area. The percentage decrease in task time for the task with the smaller area was 44.80%, 44.66%, and 47.76% for position 1, position 2, and position 3,

respectively. The percentage decrease in task time for the task with the larger area was 39.71%, 35.02%, and 31.41% for position 1, position 2, and position 3, respectively.

The experimental results showed that the motion scaling teleoperation decreased the task completion time significantly. The motion scaling provided not only delicate control but also macro movements which allowed the subjects less control over the haptic device to move the small piece of plastic approximately to the desired positions.

5.1.2 Force Feedback

The experimental results in section 4.4 showed the effect of force feedback. The variation in the maximum force data was caused by different sensitivities and reaction times between subjects. Some subjects detected the impact very soon and took proper action not to apply more force on the pipes right away. On the other hand, other subjects realized the impact slightly late, and they took proper action too late due to slow reaction time. When subjects did not pull the haptic device back to avoid the pipes, the end-effector kept applying force on the pipes. In this case, the maximum force value was higher than the former case.

Even though all the subjects had different control styles, sensitivity and reaction time, the average maximum force value for the excavating tasks decreased by 45.45% using the force feedback, and 77.67% using both force feedback and safety function. Additionally, the average maximum force value for the demolition tasks decreased by 42.46% using force feedback, and 76.36% using both force feedback and safety function.

The experimental results showed that the average maximum force values when using both force feedback and safety function were above 5 N from all subjects even though

the threshold value for the safety function was set to 5 N. During the experiment, subjects tended to rotate the bucket fast to dig up the perlite, which is why the average maximum force was above 5 N.

The experimental results from subjects 2 and 5 shown in Figure 35 and the experimental results from subjects 6 and 8 shown in Figure 36 were unusual. When the speed of the end-effector is fast, the maximum force value is usually bigger than the opposite case because it is hard to capture the moment when the end-effector first touches the buried bars. Subject 2 in Figure 35 and subject 6 in Figure 36 rotated the end-effector really fast; however subject 5 in Figure 35 and subject 8 in Figure 36 performed the excavating tasks without force feedback very carefully. Therefore, the average maximum force value without force feedback from subject 5 and 8 was less than the average maximum force value with force feedback from subject 2 and 6.

5.2 Conclusion

This study presents an innovative teleoperated motion scaling robotic arm with force feedback for the construction industry. The TMSRA enables the operators to control the slave equipment intuitively, precisely, and efficiently using motion scaling and force feedback. The TMSRA, when paired with force feedback and a safety function, helps the operator to apply less force on the buried objects, which should not be damaged in the simulated construction workspace. The average maximum force value differs between subjects, but the TMSRA with the previously mentioned functions still significantly decreases the maximum force value on an object. One of the primary benefits of using the system is the improved work efficiency, which is obtained by strategically controlling the velocity of the robotic arm in the simulated construction work. The robotic arm can reach

workspace more quickly and finish given tasks faster. For the tasks which require delicate control, the effect of the motion scaling is bigger.

The primary purpose of this research is to propose a teleoperated motion scaling robotic arm with force feedback for the construction industry. By adopting a motion scaling control system, work efficiency on construction sites could be significantly improved. This could resolve issues relating to shortages of equipment operators and delayed construction work. Also, it would contribute to generating more revenue on construction sites. The teleoperation system would reduce the number of construction site accident injuries because the operators do not need to be in the equipment so they would be safe even when unexpected accidents happen. Also, they would be free from construction dust. Adopting force feedback to the construction equipment would reduce the number of accidents relating to buried facilities by decreasing the maximum force applied to the facilities. This could save people's lives and the cost of restoration work.

There are improvements that can be made for higher work efficiency and a more reliable system. Future works will include having a new master system which allows the operator to control the slave more intuitively and efficiently. The haptic device used in this study had 6 revolute joints, but only 4 joints were used to control the physical robotic arm. While performing the experiments, the subjects wanted to fix the 2 joints in a position so that the 2 joints did not rotate. The extra 2 rotating joints distracted subjects to focus on their control. In addition to fixing the extra 2 rotating joints, the overshoot issue should be addressed. From the experiments for force feedback and safety function, the overshoot was observed. The experimental data showed that the maximum force values exceeded the

threshold value for the safety function. The overshoot should be eliminated by increasing the refresh rate between the master system and the slave system in future studies.

I contributed the following items to this Master's Thesis.

- ✓ Designed the physical robotic arm, fabricated the parts using a 3D printer and a laser cutting machine, and then assembled and tested the prototype
- ✓ Added two main functionality to the downloaded ROS packages to suit this study's purpose
  - Actuating the three actuators of the haptic device when the force information from Nano17 was received to implement force feedback
  - Control the Dynamixel motor based on the velocity control algorithm
- ✓ Created nodes to integrate the haptic device, the physical robotic arm with Nano17
  - Transmitting velocity information and button states of the haptic device
  - Processing velocity information based on the velocity information and button states of the haptic device
  - Processing velocity information based on force information from Nano 17 for the safety function
  - Reading force information of the end-effector from Nano17 and reducing the force information based on the reduction ratio
  - Transmitting the processed force information to the haptic device
- ✓ Conducted human subjects tests with 10 subjects
  - Motion Scaling Teleoperation / Force Feedback
- ✓ Analyzed the data from human subjects tests
- ✓ Wrote this thesis with help from the writing center on campus

APPENDIX A

$$M(1) = -2238.36 + x_{31} + x_{32} \times x_4 \tag{A1}$$

$$M(2) = x_{33} \tag{A2}$$

$$M(3) = x_{37} \tag{A3}$$

$$M(4) = x_{38} \tag{A3}$$

$$M(5) = x_{33} \tag{A4}$$

$$\begin{aligned} M(6) = {} & -946.763165 \\ & + x_0 \\ & \times (5504.71 \cdot x_{39} + x_{10} \cdot x_{42} + x_{10} \cdot x_{44} + x_2 + x_{41} \cdot x_6) \\ & + x_1 \times (x_{26} + x_{27} \cdot x_{39} + x_{41} \cdot x_7 + x_{42} \cdot x_6 + x_{44} \cdot x_6) \\ & - 0.1365 \cdot x_{28} + x_3 \cdot x_{45} - 0.1365 \cdot x_{45} \end{aligned} \tag{A5}$$

$$M(7) = x_{37} \tag{A6}$$

$$M(8) = x_{38} \tag{A7}$$

$$M(9) = x_{37} \tag{A8}$$

$$M(10) = x_{37} \tag{A9}$$

$$\begin{aligned} M(11) = {} & 6972.314165 + x_{36} \cdot x_{50} + x_{49} + 0.1365 \cdot x_{50} \cdot x_6 + 0.1365 \cdot \\ & x_7 \times (54134.89 \cdot x_{47} + x_{48}) \end{aligned} \tag{A10}$$

$$M(12) = x_{51} \tag{A11}$$

$$M(13) = x_{38} \tag{A12}$$

$$M(14) = x_{38} \tag{A13}$$

$$M(15) = x_{51} \tag{A14}$$

$$M(16) = 18126.077785 \tag{A15}$$

$$x_0 = \sin\theta_3 \tag{A16}$$

$$x_1 = \cos q_3 \tag{A17}$$

$$x_2 = 0.1 \times x_0 + 19051.61 \times x_1 \tag{A18}$$

$$x_3 = x_1 \times (-0.1365 \times {x_0}^2 - 0.1365 \times {x_1}^2) \tag{A19}$$

$$x_4 = -0.1365 \times \sin {q_2}^2 - 0.1365 \times \cos {q_2}^2 \tag{A20}$$

$$x_5 = x_3 + x_4 \tag{A21}$$

$$x_6 = \cos q_4 \tag{A22}$$

$$x_7 = \sin q_4 \tag{A23}$$

$$x_8 = x_0 \times x_6 + x_1 \times x_7 \tag{A24}$$

$$x_9 = x_1 \times x_6 \tag{A25}$$

$$x_{10} = -x_7 \tag{A26}$$

$$x_{11} = x_0 \times x_{10} \quad \text{(A27)}$$

$$x_{12} = x_{11} + x_9 \quad \text{(A28)}$$

$$x_{13} = 0.1 \times x_8 + 50640.91 \times x_{12} \quad \text{(A29)}$$

$$x_{14} = {x_6}^2 \quad \text{(A30)}$$

$$x_{15} = {x_7}^2 \quad \text{(A31)}$$

$$x_{16} = -0.09888 \times x_{14} - 0.09888 \times x_{15} \quad \text{(A32)}$$

$$x_{17} = x_{11} \times x_{16} + x_{16} \times x_9 \quad \text{(A33)}$$

$$x_{18} = x_{17} + x_5 \quad \text{(A34)}$$

$$x_{19} = 10297.45 \times x_{18} + x_{13} \quad \text{(A35)}$$

$$x_{20} = 50640.91 \times x_8 + 10926.75 \times x_{12} \quad \text{(A36)}$$

$$x_{21} = -19256.61 \quad \text{(A37)}$$

$$x_{22} = x_{18} \times x_{21} + x_{20} \quad \text{(A38)}$$

$$x_{23} = 10297.45 \times x_8 + x_{12} \times x_{21} \quad \text{(A39)}$$

$$x_{24} = 54134.89 \times x_{18} + x_{23} \quad \text{(A40)}$$

$$x_{25} = x_{16} \times x_{24} \quad \text{(A41)}$$

$$x_{26} = 19051.61 \times x_0 + 1047.63 \times x_1 \quad \text{(A42)}$$

$$x_{27} = -31353.36 \tag{A43}$$

$$x_{28} = -23928.01 \tag{A44}$$

$$x_{29} = 5504.71 \times x_0 + x_1 \times x_{27} \tag{A45}$$

$$x_{30} = 31920.83 \times x_5 + x_{24} + x_{29} \tag{A46}$$

$$\begin{aligned} & x_{31} \\ & = -4755.65 \\ & + x_1 \times (5504.71 \cdot x_5 + x_{10} \cdot x_{22} + x_{10} \cdot x_{25} + x_{19} \cdot 6 + x_2) \\ & + x_1 \times (x_{19} \cdot 7 + x_{22} \cdot 6 + x_{25} \cdot 6 + x_{26} + x_{27} \cdot 5) + x_{28} \cdot 4 + x_3 \cdot 30 \end{aligned} \tag{A47}$$

$$x_{32} = 29127.64 \times x_4 + x_{28} + x_{30} \tag{A48}$$

$$x_{33} = x_{31} - 0.1365 \times x_{32} \tag{A49}$$

$$x_{34} = 4482.37 \times x_8 + 48310.24 \times x_{12} \tag{A50}$$

$$x_{35} = -53775.42 \times x_8 \tag{A51}$$

$$x_{36} = 0.09888 \times x_{14} + 0.09888 \times x_{15} \tag{A52}$$

$$\begin{aligned} x_{37} = & -12365.68 \times x_0 + 17174.35 \times x_1 - 4115.992335 \times \\ & x_0 + 7340.345 \times x_{12} \times x_7 + x_{34} + x_{35} \times x_{36} + 0.1365 \times x_{35} \times x_6 \end{aligned} \tag{A53}$$

$$x_{38} = x_{34} + 0.09888 \times x_{35} \tag{A54}$$

$$x_{39} = x_3 - 0.1365 \tag{A55}$$

$$x_{40} = x_{17} + x_{39} \tag{A56}$$

$$x_{41} = 10297.45 \times x_{40} + x_{13} \tag{A57}$$

$$x_{42} = x_{20} + x_{21} \times x_{40} \tag{A58}$$

$$x_{43} = 54134.89 \times x_{40} + x_{23} \tag{A59}$$

$$x_{44} = x_{16} \times x_{43} \tag{A60}$$

$$x_{45} = 31920.83 \times x_{39} + x_{29} + x_{43} \tag{A61}$$

$$x_{46} = x_{36} + 0.1365 \times x_{6} \tag{A62}$$

$$x_{47} = 0.1365 \times x_{7} \tag{A63}$$

$$x_{48} = -10297.45 \tag{A64}$$

$$x_{49} = 13788.60 + 19256.61 \times x_{46} + x_{47} \times x_{48} \tag{A65}$$

$$x_{50} = 19256.61 + 54134.89 \times x_{46} \tag{A66}$$

$$x_{51} = x_{49} + 0.09888 \times x_{50} \tag{A67}$$

$$C(1) = dq_2 \times y_{48} \tag{A68}$$

$$C(2) = dq_2 \times (y_0 \times y_{75} + y_{74} + y_{76} + y_{88}) + dq_3 \times y_{87} \tag{A69}$$

$$C(3) = dq_2 \cdot (y_{156} + y_{158} + y_{160} + y_{76}) + dq_3 \cdot (y_{158} + y_{160} + y_{171} + y_{88}) + y_{172} \tag{A70}$$

$$C(4) = dq_2 \cdot (y_{189} + y_{191} + y_{193} + y_{76}) + dq_3 \cdot (y_{191} + y_{193} + y_{196} + y_{88}) + y_{202} \quad \text{(A71)}$$

$$C(5) = dq_2 \times y_{204} \quad \text{(A72)}$$

$$C(6) = dq_2 \cdot (y_{205} + y_{207} + y_{74} - 0.1365 \times y_{75}) + dq_2 \times y_{206} \quad \text{(A73)}$$

$$C(7) = dq_2 \cdot (y_{156} + y_{160} + y_{205} + y_{208}) + dq_3 \cdot (y_{160} + y_{171} + y_{207} + y_{208}) + y_{172} \quad \text{(A74)}$$

$$C(8) = dq_2 \cdot (y_{189} + y_{193} + y_{205} + y_{209}) + dq_3 \cdot (y_{193} + y_{196} + y_{207} + y_{209}) + y_{202} \quad \text{(A75)}$$

$$C(9) = dq_2 \times y_{222} \quad \text{(A76)}$$

$$\begin{aligned} C(10) = {} & dq_2 \cdot (31353.36 \cdot y_{58} + 4357.193295 \cdot y_{58} + y_{144} \cdot y_{59} + y_{223} \\ & + 0.1365 \cdot y_{225} \cdot y_8 + y_{225} \cdot y_{89} + y_{226} + y_{236} - y_{50} \\ & \cdot (0.1 \cdot y_{51} + 19051.61 \cdot y_{50} + 5504.71 \cdot y_{62}) + y_{51} \\ & \cdot (19051.61 \cdot y_{51} + 1047.63 \cdot y_{50} + y_{146} \cdot y_{62}) + 0.1365 \\ & \cdot y_6 \cdot (54134.89 \cdot y_{66} + y_{224} \cdot y_{55}) + 0.1365 \cdot y_{72} \\ & \cdot (5504.71 \cdot y_{51} + 31920.83 \cdot y_{62} + y_{146} \cdot y_{50})) \\ & + dq_3 \times y_{235} \end{aligned} \quad \text{(A77)}$$

$$C(11) = dq_2 \cdot (0.1365 \cdot y_{144} + y_{153} \cdot (y_{149} + y_{214}) + y_2 \cdot (17174.35 + y_{216}) + 0.1365 \cdot y_{221} + y_{226} + y_{240} + 0.1365 \cdot y_{242} \cdot y_8 + y_{242} \cdot y_{89} + y_{244} + y_{251} + 0.1365 \cdot y_6 \cdot (y_{246} + y_{248})) + dq_3 \cdot (0.1365 \cdot y_{144} + y_{153} \cdot (y_{149} + y_{231}) + y_2 \cdot (17174.35 + y_{230}) + 0.1365 \cdot y_{234} + y_{236} + y_{251} + y_{252} + 0.1365 \cdot y_{253} \cdot y_8 + y_{235} \cdot y_{89} + 0.1365 \cdot y_6 \cdot (y_{248} + y_{254})) + dq_4 \cdot y_{250} \quad \text{(A78)}$$

$$C(12) = dq_2 \cdot (y_{217} + 0.1365 \cdot y_{211} + y_{226} + y_{257} + 0.1365 \cdot y_{258} \cdot y_8 + y_{258} \cdot y_{89} + y_{262} + 0.1365 \cdot y_6 \cdot (y_{246} + y_{260})) + dq_3 \cdot (y_{232} + 0.1365 \cdot y_{234} + y_{236} + y_{262} + y_{263} + 0.1365 \cdot y_{264} \cdot y_8 + y_{264} \cdot y_{89} + 0.1365 \cdot y_6 \cdot (y_{254} + y_{260})) + dq_4 \cdot (0.1365 \cdot y_{1444} + y_{243} + y_{251} + y_{262} + y_{266} + 0.1365 \cdot y_{267} \cdot y_8 + y_{267} \cdot y_{89} + 0.1365 \cdot y_6 \cdot (-77026 + 54134.89 \cdot y_{199} - 2 \cdot y_{265})) + dq_4 \cdot y_{261} \quad \text{(A79)}$$

$$C(13) = dq_2 \times y_{268} \quad \text{(A80)}$$

$$C(14) = dq_2 \cdot (y_{223} + 0.09888 \cdot y_{225} + y_{270} + y_{271}) + dq_3 \cdot y_{269} \quad \text{(A81)}$$

$$C(15) = dq_2 \cdot (y_{240} + 0.09888 \cdot y_{242} + y_{271} + y_{273}) + dq_3 \cdot (y_{252} + 0.09888 \cdot y_{253} + y_{270} + y_{273}) + dq_4 \cdot y_{272} \quad \text{(A82)}$$

$$C(16) = dq_2 \cdot (y_{257} + 0.09888 \cdot y_{258} + y_{271} + y_{275}) + dq_3 \cdot (y_{263} + 0.09888 \cdot y_{261} + y_{270} + y_{275}) + dq_4 \cdot (y_{266} + 0.09888 \cdot y_{267} + y_{273} + y_{275}) + dq_4 \cdot y_{274} \quad \text{(A83)}$$

$$y_0 = -0.1365 \times \sin {q_2}^2 - 0.1365 \times \cos {q_2}^2 \quad \text{(A84)}$$

$$y_1 = 27125.27 \times y_0 \quad \text{(A85)}$$

$$y_2 = \sin q_3 \quad \text{(A86)}$$

$$y_3 = \cos q_3 \quad \text{(A87)}$$

$$y_4 = -12365.68 \times y_2 + 17174.35 \times y_3 \quad \text{(A88)}$$

$$y_5 = y_3 \times y_4 \quad \text{(A89)}$$

$$y_6 = \sin q_4 \quad \text{(A90)}$$

$$y_7 = -y_6 \quad \text{(A91)}$$

$$y_8 = \cos q_4 \quad \text{(A92)}$$

$$y_9 = {y_8}^2 \quad \text{(A93)}$$

$$y_{10} = {y_6}^2 \quad \text{(A94)}$$

$$y_{11} = -0.09888 \times y_{10} - 0.09888 \times y_9 \quad \text{(A95)}$$

$$y_{12} = y_3 \times y_6 \quad \text{(A96)}$$

$$y_{13} = y_{12} + y_2 \times y_8 \quad \text{(A97)}$$

$$y_{14} = -53775.42 \quad \text{(A98)}$$

$$y_{15} = y_3 \times y_8 \quad \text{(A99)}$$

$$y_{16} = y_2 \times y_7 \quad \text{(A100)}$$

$$y_{17} = y_{15} + y_{16} \quad \text{(A101)}$$

$$y_{18} = {y_{13}}^2 \times y_{14} + {y_{17}}^2 \times y_{14} \quad \text{(A102)}$$

$$y_{19} = y_{11} \times y_{18} \quad \text{(A103)}$$

$$y_{20} = y_{19} \times y_{17} + y_5 \quad \text{(A104)}$$

$$y_{21} = 4482.37 \times y_{13} + 48310.24 \times y_{17} \quad \text{(A105)}$$

$$y_{22} = y_{17} \times y_{21} \quad \text{(A106)}$$

$$y_{23} = {y_3}^2 \quad \text{(A107)}$$

$$y_{24} = {y_2}^2 \quad \text{(A108)}$$

$$y_{25} = y_{17} \times (-0.1365 \times y_{23} - 0.1365 \times y_{24}) \quad \text{(A109)}$$

$$y_{26} = y_0 + y_{25} \quad \text{(A110)}$$

$$y_{27} = y_{11} \times y_{15} + y_{11} \times y_{16} \quad \text{(A111)}$$

$$y_{28} = y_{26} + y_{27} \quad \text{(A112)}$$

$$y_{29} = 53775.42 \times y_{16} \quad \text{(A113)}$$

$$y_{30} = y_{13} \times y_{29} + y_{22} \quad \text{(A114)}$$

$$y_{31} = -y_{13} \quad \text{(A115)}$$

$$y_{32} = y_{21} \times y_{31} \quad \text{(A116)}$$

$$y_{33} = y_{17} \times y_{29} + y_{32} \quad \text{(A117)}$$

$$y_{34} = 30153.79 \times y_{26} \quad \text{(A118)}$$

$$y_{35} = y_2 \times y_{34} \quad \text{(A119)}$$

$$y_{36} = -y_2 \quad \text{(A120)}$$

$$y_{37} = y_{36} \times y_4 \quad \text{(A121)}$$

$$y_{38} = y_{19} \times y_8 + y_{37} \quad \text{(A122)}$$

$$y_{39} = y_3 \times y_{34} \quad \text{(A123)}$$

$$y_{40} = -30153.79 \quad \text{(A124)}$$

$$y_{41} = y_{23} \times y_{40} + y_{24} \times y_{40} \quad \text{(A125)}$$

$$y_{42} = y_{18} + y_{41} \quad \text{(A126)}$$

$$y_{43} = y_{25} \times y_{42} \quad \text{(A127)}$$

$$y_{44} = y_1 + y_2 \times (y_{20} + y_{30} \times y_8 + y_{33} \times y_7 + y_{35}) + y_3 \times (y_{30} \times y_6 + y_{33} \times y_8 + y_{38} + y_{39}) + y_{43} \quad \text{(A128)}$$

$$y_{45} = -27125.57 \quad \text{(A129)}$$

$$y_{46} = y_{42} + y_{45} \quad \text{(A130)}$$

$$y_{47} = y_0 \times y_{46} \quad \text{(A131)}$$

$$y_{48} = y_{44} + y_{47} \quad \text{(A132)}$$

$$y_{49} = -y_0 - 0.1365 \quad \text{(A133)}$$

$$y_{50} = 2 \times y_3 \quad \text{(A134)}$$

$$y_{50} = 2 \times y_3 \quad \text{(A135)}$$

$$y_{52} = -12365.68 \times y_{51} + 17174.35 \times y_{51} \quad \text{(A136)}$$

$$y_{53} = y_{50} \times y_8 \quad \text{(A137)}$$

$$y_{54} = y_{51} \times y_7 \quad \text{(A138)}$$

$$y_{55} = y_{53} + y_{54} \quad \text{(A139)}$$

$$y_{56} = y_{50} \times y_6 + y_{51} \times y_8 \quad \text{(A140)}$$

$$y_{57} = 4482.37 \times y_{56} + 48310.24 \times y_{55} \quad \text{(A141)}$$

$$y_{58} = y_{36} \times y_{49} \quad \text{(A142)}$$

$$y_{59} = y_3 \times y_{49} \quad \text{(A143)}$$

$$y_{60} = y_{58} \times y_8 + y_{59} \times y_7 \quad \text{(A144)}$$

$$y_{61} = y_0 - 0.1365 \quad \text{(A145)}$$

$$y_{62} = 2 \times y_{25} + y_{61} \quad \text{(A146)}$$

$$y_{63} = y_{11} \times y_{53} + y_{11} \times y_{54} + y_{62} \quad \text{(A147)}$$

$$y_{64} = 53775.42 \times y_{63} \quad \text{(A148)}$$

$$y_{65} = y_{14} \times y_{60} + y_{55} \times y_{57} + y_{56} \times y_{64} \quad \text{(A149)}$$

$$y_{66} = y_{58} \times y_6 + y_{59} \times y_8 \quad \text{(A150)}$$

$$y_{67} = -y_{56} \quad \text{(A151)}$$

$$y_{68} = 53775.42 \times y_{66} + y_{55} \times y_{64} + y_{57} \times y_{67} \quad \text{(A152)}$$

$$y_{69} = 30153.79 \times y_8 \quad \text{(A153)}$$

$$y_{70} = y_{14} \times {y_{55}}^2 + y_{14} \times {y_{56}}^2 \quad \text{(A154)}$$

$$y_{71} = y_{11} \times y_{70} \quad \text{(A155)}$$

$$y_{72} = -y_{58} \quad \text{(A156)}$$

$$y_{73} = y_{40} \times {y_{50}}^2 + y_{40} \times {y_{51}}^2 + y_{70} \quad \text{(A157)}$$

$$y_{74} = 27125.57 \cdot y_{49} + 54251.14 \cdot y_{61} + y_2 \cdot (y_{40} \cdot y_{58} + y_{50} \cdot y_{52} + y_{51} \cdot y_{69} + y_{65} \cdot y_8 + y_{68} \cdot y_7 + y_7 \cdot y_{71}) + y_{25} \cdot y_{73} + y_{73} \cdot (30153.79 \cdot y_{59} + y_{50} \cdot y_{69} + y_{52} \cdot y_{72} + y_6 \cdot y_{65} + y_{68} \cdot y_8 + y_{71} \cdot y_8) \quad \text{(A158)}$$

$$y_{75} = -108502.28 + y_{73} \quad \text{(A159)}$$

$$y_{76} = -y_{48} \quad \text{(A160)}$$

$$y_{77} = -3702.6 \quad \text{(A161)}$$

$$y_{78} = y_{25} - 0.1365 \quad \text{(A162)}$$

$$y_{79} = y_{25} + y_{78} \quad \text{(A163)}$$

$$y_{80} = 53775.42 \times y_{79} \quad \text{(A164)}$$

$$y_{81} = y_{13} \times y_{80} + y_{22} \quad \text{(A165)}$$

$$y_{82} = y_{17} \times y_{80} + y_{32} \quad \text{(A166)}$$

$$y_{83} = 30153.79 \times y_{78} \quad \text{(A167)}$$

$$y_{84} = y_2 \times y_{83} \quad \text{(A168)}$$

$$y_{85} = y_3 \times y_{83} \quad \text{(A169)}$$

$$y_{86} = y_2 \cdot (y_{20} + y_7 \cdot y_{82} + y_8 \cdot y_{81} + y_{84}) + y_3 \cdot (y_{38} + y_6 \cdot y_{81} + y_8 \cdot y_{82} + y_{85}) + y_{43} + y_{77} \quad \text{(A170)}$$

$$y_{87} = y_{47} + y_{86} \quad \text{(A171)}$$

$$y_{88} = -y_{87} \quad \text{(A172)}$$

$$y_{89} = 0.09888 \times y_{10} + 0.09888 \times y_{9} \quad \text{(A173)}$$

$$y_{90} = 0.1365 \times y_{8} + y_{89} \quad \text{(A174)}$$

$$y_{91} = 10297.45 \times y_{13} \quad \text{(A175)}$$

$$y_{92} = -19256.61 \quad \text{(A176)}$$

$$y_{93} = y_{17} \times y_{92} + y_{91} \quad \text{(A177)}$$

$$y_{94} = 54134.89 \times y_{28} \quad \text{(A178)}$$

$$y_{95} = y_{93} + y_{94} \quad \text{(A179)}$$

$$y_{96} = 54134.89 \times y_{90} \quad \text{(A180)}$$

$$y_{97} = 19256.61 + y_{96} \quad \text{(A181)}$$

$$y_{98} = 53775.42 + y_{31} \quad \text{(A182)}$$

$$y_{99} = y_{97} + y_{98} \quad \text{(A183)}$$

$$y_{100} = -y_{93} \quad \text{(A184)}$$

$$y_{101} = 50640.91 \times y_{13} \quad \text{(A185)}$$

$$y_{102} = 10926.75 \times y_{17} \quad \text{(A186)}$$

$$y_{103} = -y_{101} - y_{102} \quad \text{(A187)}$$

$$y_{104} = 19256.61 \times y_{28} + y_{103} \quad \text{(A188)}$$

$$y_{105} = -48310.24 \quad \text{(A189)}$$

$$y_{106} = 0.1365 \times y_{6} \quad \text{(A190)}$$

$$y_{107} = y_{105} + y_{106} \times y_{14} \quad \text{(A191)}$$

$$y_{108} = y_{15} + y_{36} \times y_{6} \quad \text{(A192)}$$

$$y_{109} = y_{36} \times y_{8} \quad \text{(A193)}$$

$$y_{110} = -y_{12} \quad \text{(A194)}$$

$$y_{111} = y_{109} + y_{1110} \quad \text{(A195)}$$

$$y_{112} = 0.1365 \times y_{2} \quad \text{(A196)}$$

$$y_{113} = y_{109} \times y_{11} + y_{112} + y_{11} \times y_{110} \quad \text{(A197)}$$

$$y_{114} = -10297.45 \quad \text{(A198)}$$

$$y_{115} = 13788.6 + y_{21} \quad \text{(A199)}$$

$$y_{116} = 19256.61 \times y_{90} + y_{106} \times y_{114} + y_{115} \quad \text{(A200)}$$

$$y_{117} = 0.1 \times y_{108} + 50640.91 \times y_{111} + 10297.45 \times y_{113} + y_{107} + y_{116} \times y_{17} \quad \text{(A201)}$$

$$y_{118} = y_{100} \times y_{99} + y_{104} + y_{117} + y_{90} \times y_{95} \quad \text{(A202)}$$

$$y_{119} = 31353.36 + 30153.79 \times y_{36} + 4357.1933 \quad \text{(A203)}$$

$$y_{120} = -y_{119} \quad \text{(A204)}$$

$$y_{121} = 0.1 \times y_{13} \quad \text{(A205)}$$

$$y_{122} = 50640.91 \times y_{17} \quad \text{(A206)}$$

$$y_{123} = y_{121} + y_{122} \quad \text{(A207)}$$

$$y_{124} = 10297.45 \times y_{28} \quad \text{(A208)}$$

$$y_{125} = y_{123} + y_{124} \quad \text{(A209)}$$

$$y_{126} = 54137.89 \times y_{106} \quad \text{(A210)}$$

$$y_{127} = y_{114} + y_{126} \quad \text{(A211)}$$

$$y_{128} = 53775.42 \times y_{17} \quad \text{(A212)}$$

$$y_{129} = y_{127} + y_{128} \quad \text{(A213)}$$

$$y_{130} = -y_{106} \quad \text{(A214)}$$

$$y_{131} = 4482.37 + y_{14} \times y_{90} \quad \text{(A215)}$$

$$y_{132} = 50640.91 \times y_{108} + 10926.75 \times y_{111} + y_{113} \times y_{92} + y_{116} \times y_{31} + y_{131} \quad \text{(A216)}$$

$$y_{133} = y_{125} + y_{129} \times y_{28} + y_{130} \times y_{95} + y_{132} \quad \text{(A217)}$$

$$y_{134} = 31920.83 \times y_{26} \quad \text{(A218)}$$

$$y_{135} = -17174.35 \quad \text{(A219)}$$

$$y_{136} = 2097.8 + y_4 \quad \text{(A220)}$$

$$y_{137} = 19051.61 \times y_2 \quad \text{(A221)}$$

$$y_{138} = 1047.63 \times y_3 \quad \text{(A222)}$$

$$y_{139} = 5504.71 \times y_2 \quad \text{(A223)}$$

$$y_{140} = -y_{17} \quad \text{(A224)}$$

$$y_{141} = 10297.45 \cdot y_{108} + 54134.89 \cdot y_{113} + y_{111} \cdot y_{92} + y_{129} \cdot y_{140} + y_{13} \cdot y_{99} \quad \text{(A225)}$$

$$y_{142} = y_{11} \times y_{141} \quad \text{(A226)}$$

$$y_{143} = 0.1 \times y_3 + 19051.61 \times y_{36} - 4279.7 \times y_3 + 5504.71 \times y_{112} + y_{135} + y_{136} \times 3 - y_{137} - y_{138} + 0.1365 \times y_{139} + y_{142} \times y_7 \quad \text{(A227)}$$

$$y_{144} = -5504.71 \quad \text{(A228)}$$

$$y_{145} = 30153.79 \times y_3 + y_{144} \quad \text{(A229)}$$

$$y_{146} = -31353.36 \quad \text{(A230)}$$

$$y_{147} = 19051.61 \times y_3 \tag{A231}$$

$$y_{148} = -4116.99 \tag{A232}$$

$$y_{149} = -123665.68 + y_{115} \tag{A233}$$

$$y_{150} = 0.1 \times y_2 \tag{A234}$$

$$y_{151} = 1047.63 \times y_{36} + y_{112} \times y_{146} + y_{136} \times y_{36} + y_{142} \times y_8 + 2 \times y_{147} + y_{149} + y_{150} \tag{A235}$$

$$y_{152} = 5504.71 \times y_{26} \tag{A236}$$

$$y_{153} = -y_3 \tag{A237}$$

$$y_{154} = 5504.71 \times y_3 + 30153.79 \times y_{112} + y_{141} + y_{145} \times y_{153} + y_{146} \times y_{36} \tag{A238}$$

$$y_{155} = y_{154} \times y_{25} \tag{A239}$$

$$y_{156} = y_1 + y_{155} + y_2 \cdot (31353.36 \cdot y_{26} + y_{118} \cdot y_8 + y_{120} \cdot y_{26} + y_{133} \cdot y_7 + 0.1365 \cdot y_{134} + y_{143}) + y_3 \cdot (y_{118} \cdot y_6 + y_{133} \cdot y_8 + y_{145} \cdot y_{26} + y_{151} + y_{152}) \tag{A240}$$

$$y_{157} = y_{254} + y_{45} \tag{A241}$$

$$y_{158} = y_0 \times y_{157} \tag{A242}$$

$$y_{159} = y_2 \times (y_{107} \times y_8 + y_{131} \times y_7 + y_{135}) + y_3 \times (y_{107} \times y_6 + y_{131} \times y_8 + y_{149}) \quad \text{(A243)}$$

$$y_{160} = -y_{159} \quad \text{(A244)}$$

$$y_{161} = 54134.89 \times y_{79} \quad \text{(A245)}$$

$$y_{162} = y_{161} + y_{93} \quad \text{(A246)}$$

$$y_{163} = -y_{79} \quad \text{(A247)}$$

$$y_{164} = 19256.61 \times y_{79} + y_{103} \quad \text{(A248)}$$

$$y_{165} = y_{117} + y_{162} \times y_{90} + y_{163} \times y_{99} + y_{164} \quad \text{(A249)}$$

$$y_{166} = 10297.45 \times y_{79} \quad \text{(A250)}$$

$$y_{167} = y_{123} \times y_{166} \quad \text{(A251)}$$

$$y_{168} = y_{129} \times y_{79} + y_{130} \times y_{162} + y_{132} \times y_{167} \quad \text{(A252)}$$

$$y_{169} = 31920.83 \times y_{78} \quad \text{(A253)}$$

$$y_{170} = 5504.71 \times y_{78} \quad \text{(A254)}$$

$$y_{171} = y_{155} + y_2 \cdot (31353.36 \cdot y_{78} + y_{120} \cdot y_{78} + y_{143} + y_{135} \cdot y_8 + y_{168} \cdot y_7 + 0.1365 \cdot y_{169}) + y_3 \cdot (y_{145} \cdot y_{78} + y_{151} + y_{165} \cdot y_6 + y_{168} \cdot y_8 + y_{170}) + y_{77} \quad \text{(A255)}$$

$$y_{172} = dq_4 \times y_{159} \tag{A256}$$

$$y_{173} = 24609.47 + y_{98} \tag{A257}$$

$$y_{174} = 0.09888 \times y_{13} \tag{A258}$$

$$y_{175} = 1904.09 + y_{115} \tag{A259}$$

$$y_{176} = 0.1 \times y_{17} + 50640.91 \times y_{31} - 1904.09 \times y_{17} + 10297.45 \times y_{174} + y_{105} + y_{175} \times y_{17} + 0.09888 \times y_{91} \tag{A260}$$

$$y_{177} = y_{100} \times y_{173} + y_{104} + y_{176} + 0.09888 \times y_{94} \tag{A261}$$

$$y_{178} = y_{114} + y_{128} \tag{A262}$$

$$y_{179} = -5317.31 \tag{A263}$$

$$y_{180} = 4482.37 + y_{179} \tag{A264}$$

$$y_{181} = 10926.75 \times y_{31} + y_{121} + 2 \times y_{122} + y_{174} \times y_{92} + y_{175} \times y_{31} + y_{180} \tag{A265}$$

$$y_{182} = y_{124} + y_{178} \times y_{28} + y_{181} \tag{A266}$$

$$y_{183} = 10297.45 \cdot y_{17} + 54134.89 \cdot y_{174} + y_{13} \cdot y_{173} + y_{140} \cdot y_{178} + y_{31} \cdot y_{92} \tag{A267}$$

$$y_{184} = y_{11} \times y_{183} \tag{A268}$$

$$y_{185} = y_{184} \times y_7 + y_5 \tag{A269}$$

$$y_{186} = y_{184} \times y_8 + y_{37} \tag{A270}$$

$$y_{187} = y_{183} + y_{41} \tag{A271}$$

$$y_{188} = y_{187} \times y_{25} \tag{A272}$$

$$y_{189} = y_1 + y_{188} + y_2 \times (y_{177} \times y_8 + y_{182} \times y_7 + y_{185} + y_{35}) + y_3 \times (y_{177} \times y_6 + y_{182} \times y_8 + y_{186} + y_{39}) \tag{A273}$$

$$y_{190} = y_{187} + y_{45} \tag{A274}$$

$$y_{191} = y_0 \times y_{190} \tag{A275}$$

$$y_{192} = y_2 \times (y_{105} \times y_8 + y_{180} \times y_7) + y_3 \times (y_{105} \times y_6 + y_{180} \times y_8) \tag{A276}$$

$$y_{193} = -y_{192} \tag{A277}$$

$$y_{194} = 0.09888 \times y_{161} + y_{163} \times y_{173} + y_{164} \times y_{176} \tag{A278}$$

$$y_{195} = y_{166} + y_{178} \times y_{79} + y_{181} \tag{A279}$$

$$y_{196} = y_{188} + y_2 \times (y_{185} + y_{194} \times y_8 + y_{195} \times y_7 + y_{84}) + y_3 \times (y_{186} + y_{194} \times y_6 + y_{195} \times y_8 + y_{85}) + y_{77} \tag{A280}$$

$$y_{197} = 53775.42 \times y_{106} \tag{A281}$$

$$y_{198} = -193240.96 + y_{130} \times y_{14} - 2 \times y_{115} \tag{A282}$$

$$y_{199} = y_{90} - 0.09888 \tag{A283}$$

$$y_{200} = y_{90} + 0.09888 \tag{A284}$$

$$y_{201} = 17929.48 + 53775.42 \times y_{199} - 107550.84 \times y_{200} \tag{A285}$$

$$y_{202} = dq_4 \times \big(y_{160} + y_{193} + y_{114} \times (y_{135} + y_{198} \times y_8 + y_{201} \times y_7) + y_3 \times (y_{149} + y_{198} \times y_6 + y_{201} \times y_8)\big) + dq_4 \times y_{192} \tag{A286}$$

$$y_{203} = -0.1365 \times y_{46} \tag{A287}$$

$$y_{204} = y_{203} + y_{44} \tag{A288}$$

$$y_{205} = -y_{204} \tag{A289}$$

$$y_{206} = y_{203} + y_{86} \tag{A290}$$

$$y_{207} = -y_{206} \tag{A291}$$

$$y_{208} = -0.1365 \times y_{157} \tag{A292}$$

$$y_{209} = -0.1365 \times y_{190} \tag{A293}$$

$$y_{210} = y_{101} + y_{102} \tag{A294}$$

$$y_{211} = y_{210} + y_{28} \times y_{92} \tag{A295}$$

$$y_{212} = y_{125} \times y_{140} + y_{13} \times y_{211} \tag{A296}$$

$$y_{213} = y_{147} + y_{150} \tag{A297}$$

$$y_{214} = y_{152} + y_{213} \tag{A298}$$

$$y_{215} = y_{137} + y_{138} \tag{A299}$$

$$y_{216} = y_{146} \times y_{26} + y_{215} \tag{A300}$$

$$y_{217} = y_{153} \times y_{214} + y_2 \times y_{216} \tag{A301}$$

$$y_{218} = y_{31} \times y_{95} \tag{A302}$$

$$y_{219} = y_{17} \times y_{95} \tag{A303}$$

$$y_{220} = y_{139} + y_{146} \times 3 \tag{A304}$$

$$y_{221} = y_{36} \times (y_{134} + y_{220}) \tag{A305}$$

$$y_{222} = y_{212} + y_{217} + 0.1365 \times y_{218} \times y_8 + y_{218} \times y_{89} + 0.1365 \times y_{219} \times y_6 + 0.1365 \times y_{221} \tag{A306}$$

$$y_{223} = 19256.61 \times y_{60} + y_{114} \times y_{66} - y_{115} \times (0.1 \times y_{56} + 50640.91 \times y_{55} + 10297.45 \times y_{63}) + y_{56} \times (5064.91 \times y_{56} + 10926.75 \times y_{55} + y_{92} \times y_{63}) \tag{A307}$$

$$y_{224} = 10297.45 \times y_{56} + 54134.89 \times y_{63} + y_{55} \times y_{92} \tag{A308}$$

$$y_{225} = 54134.89 \times y_{60} + y_{224} \times y_{67} \tag{A309}$$

$$y_{226} = -y_{115} \tag{A310}$$

$$y_{227} = y_{210} + y_{79} \times y_{92} \tag{A311}$$

$$y_{228} = y_{13} \times y_{227} + y_{140} \times y_{167} \tag{A312}$$

$$y_{229} = y_{162} \times y_{31} \tag{A313}$$

$$y_{230} = y_{146} \times y_{78} + y_{215} \tag{A314}$$

$$y_{231} = y_{170} + y_{213} \tag{A315}$$

$$y_{232} = y_{153} \times y_{231} + y_2 \times y_{230} \tag{A316}$$

$$y_{233} = y_{162} \times y_{17} \tag{A317}$$

$$y_{234} = y_{36} \times (y_{169} + y_{220}) \tag{A318}$$

$$y_{235} = y_{228} + 0.1365 \times y_{229} \times y_8 + y_{229} \times y_{89} + y_{232} + 0.1365 \times y_{233} \times y_6 + 0.1365 \times y_{234} \tag{A319}$$

$$y_{236} = -y_{235} \tag{A320}$$

$$y_{237} = 48310.24 + y_{115} \tag{A321}$$

$$y_{238} = -y_{90} \tag{A322}$$

$$y_{239} = 4482.37 \times y_{108} + 48310.24 \times y_{111} + y_{106} \times y_{99} + y_{129} \times y_{238} \tag{A323}$$

$$y_{240} = y_{13} \times (y_{211} + y_{237}) + y_{140} \times (y_{125} + y_{131}) + y_{239} \tag{A324}$$

$$y_{241} = y_{108} \times y_{14} + y_{129} \tag{A325}$$

$$y_{242} = y_{218} + y_{241} \tag{A326}$$

$$y_{243} = 751.39 \tag{A327}$$

$$y_{244} = -12365.68 \times y_3 + 17174.35 \times y_{36} + y_{148} \times y_3 + y_{243} \quad \text{(A328)}$$

$$y_{245} = 53775.42 \times y_{13} \quad \text{(A329)}$$

$$y_{246} = y_{219} + y_{245} \quad \text{(A330)}$$

$$y_{247} = y_{92} - y_{96} \quad \text{(A331)}$$

$$y_{248} = 53775.42 \times y_{111} + y_{247} \quad \text{(A332)}$$

$$y_{249} = y_{106} \times y_{97} + y_{127} \times y_{238} \quad \text{(A333)}$$

$$y_{250} = 0.1365 \times y_{127} \times y_8 + y_{127} \times y_8 + 0.1365 \times y_{144} + y_{243} + 0.1365 \times y_{247} \times y_6 + y_{249} \quad \text{(A334)}$$

$$y_{251} = -y_{250} \quad \text{(A335)}$$

$$y_{252} = y_{13} \times (y_{227} + y_{237}) + y_{140} \times (y_{131} + y_{167}) + y_{239} \quad \text{(A336)}$$

$$y_{253} = y_{229} + y_{241} \quad \text{(A337)}$$

$$y_{254} = y_{233} + y_{245} \quad \text{(A338)}$$

$$y_{255} = 1018.21 \quad \text{(A339)}$$

$$y_{256} = 4482.37 \times y_{17} + 48310.24 \times y_{31} + y_{17} \times y_{179} + y_{255} \quad \text{(A340)}$$

$$y_{257} = y_{13} \times (48310.24 + y_{211}) + y_{140} \times (y_{125} + y_{180}) + y_{256} \quad \text{(A341)}$$

$$y_{258} = y_{114} + y_{218} \quad \text{(A342)}$$

$$y_{259} = -5352.86 + y_{92} \tag{A343}$$

$$y_{260} = y_{259} + y_{98} \tag{A344}$$

$$y_{261} = 0.1365 \times (y_{227} \times y_{237}) + y_{140} \times (y_{167} + y_{180}) + y_{256} \tag{A345}$$

$$y_{262} = -y_{261} \tag{A346}$$

$$y_{263} = y_{13} \times (48310.24 + y_{227}) + y_{140} \times (y_{167} + y_{180}) + y_{256} \tag{A347}$$

$$y_{264} = y_{114} + y_{229} \tag{A348}$$

$$y_{265} = 54134.89 \times y_{200} \tag{A349}$$

$$y_{266} = 19256.61 \times 130 + y_{106} \times (38513.22 + y_{265}) + y_{114} \times y_{199} - y_{200} \times (-2 \times 10297.45 + y_{126}) \tag{A350}$$

$$y_{267} = 41189.8 + 54134.89 \times y_{130} + 2 \times y_{126} \tag{A351}$$

$$y_{268} = y_{212} + 0.09888 \times y_{218} \tag{A352}$$

$$y_{269} = y_{228} + 0.09888 \times y_{229} \tag{A353}$$

$$y_{270} = -y_{269} \tag{A354}$$

$$y_{271} = -y_{268} \tag{A355}$$

$$y_{272} = 0.09888 \times y_{127} + y_{249} \tag{A356}$$

$$y_{273} = -y_{272} \tag{A357}$$

$$y_{274} = 0.09888 \times y_{114} + y_{255} \tag{A358}$$

$$y_{275} = -y_{274} \tag{A359}$$

$$G(1) = z_{11} \tag{A360}$$

$$G(2) = z_{11} \tag{A361}$$

$$\begin{aligned} G(3) = {} & 31353.36 \times z_5 - 5504.71 \times z_1 + 4357.2 \times z_5 \\ & + 7389.41 \times z_2 \times z_9 + z_{12} + 0.1365 \times z_{13} \times z_6 \\ & + z_{13} \times (0.09888 \times {z_2}^2 + 0.09888 \times {z_6}^2 \end{aligned} \tag{A362}$$

$$G(4) = z_{12} + 0.09888 \times y_{13} \tag{A363}$$

$$z_0 = \sin q_3 \tag{A364}$$

$$z_1 = 9.81 \times z_0 \tag{A365}$$

$$z_2 = \sin q_4 \tag{A366}$$

$$z_3 = -z_2 \tag{A367}$$

$$z_4 = \cos q_3 \tag{A368}$$

$$z_5 = 9.81 \times z_4 \tag{A369}$$

$$z_6 = \cos q_4 \tag{A370}$$

$$z_7 = x_1 \times x_3 + x_5 \times x_6 \tag{A371}$$

$$z_8 = -53775.42 \times z_7 \tag{A372}$$

$$z_9 = x_1 \times x_6 + x_2 \times x_5 \tag{A373}$$

$$z_{10} = 53775.42 \times z_9 \tag{A374}$$

$$z_{11} = z_{10} \times (-30153.79 \times y_5 + x_{10} \times x_3 + x_6 \times x_8) + z_4 \times (30153.79 \times z_1 + x_{10} \times x_6 + x_2 \times x_8) \tag{A375}$$

$$z_{12} = 19256.61 \times z_7 - 10297.45 \times z_9 \tag{A376}$$

$$z_{13} = 54134.89 \times z_7 \tag{A377}$$

REFERENCES

[1] Bureau of Labor Statistics, U.S. Daprtment of Labor, Occupational Outlook Handbook, Construction Equipment Operators on the Internet at https://www.bls.gov/ooh/construction-and-extraction/construction-equipment-operators.htm (Accessed Mar 7,2020)

[2] T. Wahng., "U.S. Construction Industry – Statistics & Facts" URL https://www.statista.com/topics/974/confstruction/#dossierSummary__chapter1 (Accessed Mar 7, 2020)

[3] Rajat Agarwal, Shankar Chandrasekaran, and Mukund Sridhar., "U.S. Construction Industry – Statistics & Facts" URL https://www.mckinsey.com/industries/capital-projects-and-infrastructure/our-insights/imagining-constructions-digital-future (Accessed Mar 9, 2020)

[4] Common Ground Alliance., "2018 DIRT Report" URL: https://commongroundalliance.com/sites/default/files/publications/2018%20DIRT%20Report%20Final_100419.pdf (Accessed Dec 17, 2019)

[5] Bujak-Pietrek S, Szadkowska-Stańczyk I. Dust exposure assessment among construction workers in Poland, 2001-2005. Med Pr 2009;60(4):247-57.

[6] McLean D, Glass B, 't Mannetje A, Douwes J. Exposure to respirable crystalline silica in the construction industry-do we have a problem? N Z Med J 2017;130(1466):78-82.

[7] Blanc PD, Toren K. Occupation in chronic obstructive pulmonary disease and chronic bronchitis: an update [State of the Art Series. Occupational lung disease in high-and lowincome countries, Edited by M. Chan-Yeung. Number 2 in the series]. The International Journal of Tuberculosis and Lung Disease 2007;11(3):251-7.

[8] Health and Safety Executive., "Construction dust CIS36" URL: https://www.hse.gov.uk/pubns/cis36.pdf (Assessed Dec 11, 2019)

[9] FMI Corporation., "FMI's Construction outlook – 2nd Quarter 2019 Report" URL: https://www.statista.com/statistics/226368/projected-value-of-total-us-construction/

[10] Tavakol E, Azari M, Zendehdel R, et al. Risk Evaluation of Construction Workers' Exposure to Silica Dust and the Possible Lung Function Impairments. Tanaffos. 2017;16(4):295–303.

[11] Occupational Safety & Health Administration., "Crystalline Silica Exposure" URL: https://www.osha.gov/Publications/osha3176.html (Assessed Dec 11, 2019)

[12] McKinsey Digital, "Construction's going digital", URL: https://medium.com/digital-mckinsey/constructions-going-digital-d8280eadb4df (Accessed Mar 9, 2020).

[13] Q.H. Le, Y.M. Jeong, C.T. Nguyen, S.Y. Yang, Development of a virtual excavatorusing SimMechanics and SymHydraulic, Journal of Drive and Control 10 (1) (2013)29–36.

[14] Q.H. Le, C.S. Jeong, H.K. Kim, H.L. Yang, S.Y. Yang, Study on modeling and controlof excavator, in: M.Y. Cho, K. Varghese, F. van Gassel (Eds.), Proceedings of the28th ISARC, pp. 969–974.

[15] Y.J. Nam, M.K. Park, Virtual excavator simulator featuring HILS and haptic joysticks, J. Mech. Sci. Technol. 29 (1) (2015) 397–407.

[16] S. Tafazoli, S. E. Salcudean, K. Hashtrudi-Zaad and P. D. Lawrence," Impedance control of a teleoperated excavator," in IEEE Transactions on Control Systems Technology, vol. 10, no. 3, pp. 355-367, May 2002.

[17] S. P. DiMaio, S. E. Salcudean, C. Reboulet, S. Tafazoli and K. Hashtrudi-Zaad," A virtual excavator for controller development and evaluation," Proceedings. 1998 IEEE International Conference on Robotics and Automation (Cat. No.98CH36146), Leuven, Belgium, 1998, pp. 52-58 vol.1.

[18] Sun, D & Lee, S & Lee, Y & Kim, S & Ueda, J & Cho, Yong & Ahn, Yong Han. (2019). Assessments of Intuition and Efficiency: Remote Control of the Arm of Excavator in Operational Space.

[19] Federico Morosi, Marco Rossoni, Giandomenico Caruso, Coordinated control paradigm for hydraulic excavator with haptic device, Automation in Construction, Volume 105, 2019, 102848.

[20] S.Y. Yang, S.J. Jin, S.K. Kwon, Remote control system of industrial field robot, in:J.J. Lee, X. Yu (Eds.), INDIN 6th IEEE International Conference on Industrial Informatics, 13–16 Jul 2008, pp. 442–447.

[21] H. Yamada, T. Muto, G. Ohashi, Development of a telerobotics system for construction robot using virtual reality, Proceedings of European Control Conference (ECC), 1999, pp. 2975–2979.

[22] H. Yamada, T. Muto, Development of a hydraulic tele-operated construction robotusing virtual reality - new master-slave control method and an evaluation of a visual feedback system, Int. J. Fluid Power 4 (2003) 35–42.

[23] H. Yamada, T. Muto, Construction tele-robotic system with virtual reality (CGpresentation 2975–2979 of virtual robot and task object using stereo vision system), Control. Intell. Syst. 35 (3) (2007) 195–201.

[24] N.R. Parker, S.E. Salcudean, P.D. Lawrence, Application of force feedback to heavy duty hydraulic machines, in: W. Book (Ed.), Proc. IEEE Conf. on Robotics and Automation (Print ISBN: 0818634502), 2–6 May 1993, pp. 375–381.

[25] P.D. Lawrence, S.E. Salcudean, N. Sepehri, D. Chan, S. Bachmann, N. Parker,M. Zhu, R. Frenette, Coordinated and force-feedback control of hydraulic ex-cavators, in: O. Khatib, J.K. Salisbury (Eds.), Experimental Robotics IV. Lecture Notes in Control and Information Sciences, 223 Springer, Heidelberg, Berlin, 1997, pp. 181–194.

[26] D. Kim, K.W. Oh, C.F. Lee, D. Hong, Novel design of haptic devices for bilateralteleoperated excavators using the wave-variable method, Int. J. Precis. Eng. Manuf.14 (2) (2013) 223–230.

[27] F.G. Frankel, Development of a Haptic Backhoe Testbed (M.S. Thesis), School of Mechanical Engineering, Georgia Institute of Technology, 13 May 2004.

[28] S. Lichiardopol, "A survey on teleoperation," Technische Universitat Eindhoven, DCT report, 2007.

[29] J. Batlle, P. Ridao, and J. Salvi, "Integration of a teleoperated robotic arm with vision systems using CORBA compatible software," in Proc. 30th Int. Symp. Automot. Technol. and Autom., Florence, Italy, Jun. 1997, pp. 371–378.

[30] Meli, Leonardo & Pacchierotti, Claudio & Prattichizzo, Domenico. (2017). Experimental evaluation of magnified haptic feedback for robot-assisted needle insertion and palpation. The International Journal of Medical Robotics and Computer Assisted Surgery. 13. E1809. 10.1002/rcs.1809.

[31] J. Wright, A. Trebi-Ollennu, F. Hartman, B. Cooper, S. Maxwell, J. Yen, and J. Morrison, "Driving a rover on mars using the rover sequencing and visualization program," in International Conference on Instrumentation, Control and Information Technology, 2005.

[32] R. R. Murphy, "Trial by fire [rescue robots]," IEEE Robotics & Automation Magazine, vol. 11, no. 3, pp. 50–61, 2004

[33] G. De Cubber, H. Balta, and C. Lietart, "Teodor: A semi-autonomous search and rescue and demining robot," in Applied Mechanics and Materials, vol. 658. Trans Tech Publ, 2014, pp. 599–605.

[34] W. Wei and Y. Kui, "Teleoperated manipulator for leak detection of sealed radioactive sources," in IEEE International Conference on Robotics and Automation (ICRA), vol. 2. IEEE, 2004, pp. 1682–1687.

[35] Caterpillar Official Website., "Caterpillar Small Excavator 311F L RR" URL https://www.cat.com/en_US/products/new/equipment/excavators/small-excavators/1000026569.html (Accessed Dec 27, 2019)

[36] Caterpillar Official Website., “Caterpillar Attachments” URL https://www.cat.com/en_US/products/new/attachments.html (Accessed Dec 27, 2019)

[37] Craig, J.J., Introduction to Robotics-Mechanics and Control, Addison-Wesley, Reading, MA, 1986

[38] E. Bayo, A finite-element approach to control the end-point motion of a single-link flexible robot. J. Robot. Syst. 4, 63–75, 1987

[39] P. Corke, ‘‘A robotics toolbox for MATLAB,’’ IEEE Robot. Autom. Mag., vol. 3, pp. 24–32, Sept. 1996.

[40] 3D SYSTEMS., “3D Systems™ Haptic Device User Guide” URL https://www.3dsystems.com/sites/default/files/2017-12/3DSystems-Touch-UserGuide.pdf (Accessed Dec 23, 2019)

[41] Korte, Christopher & Nair, Sudhesh & Nistor, Vasile & Low, Thomas & Doarn, Charles & Schaffner, Grant. (2014). Determining the Threshold of Time-Delay for Teleoperation Accuracy and Efficiency in Relation to Telesurgery. Telemedicine journal and e-health : the official journal of the American Telemedicine Association. 20. 10.1089/tmj.2013.0367.

[42] W. Garage., “ROS:Robot Operating System, 2011” URL: https://www.ros.org (Assessed Dec 17, 2019)

[43] Bruno Guilhermo de Barros Valério,. “PhantomOmni” URL https://gitlab.com/gscar-coppe-ufrj/ros/PhantomOmni (Accessed Dec 17, 2019)

[44] Darby Lim,. “Dynamixel Workbench” URL https://github.com/ROBOTIS-GIT/dynamixel-workbench (Accessed Dec 17, 2019)

[45] Derek King,. “netft utils” URL: https://github.com/UTNuclearRobotics\-Public/netft_utils (Accessed Feb 19, 2020).

[46] J. Batlle, P. Ridao, and J. Salvi, “Integration of a teleoperated robotic arm with vision systems using CORBA compatible software,” in Proc.30th Int. Symp. Automot. Technol. and Autom., Florence, Italy, Jun. 1997, pp. 371–378.

[47] H. Kobayashi and H. Nakamura. "A scaled teleoperation. " In IEEE Int"l. Workshop on Robot and Human Communication, pp: 269-274, Tokyo, Japan, September 1992.

[48] N.R. Parker, S.E. Salcudean, and P.D. Lawrence. Application of Force Feedback t.0 Heavy Duty Hydraulic Machines. In Proc. IEEE Int. Conf. on Rob. And Auto.. pages 375- 381, Atlanta, USA, May 1993.

[49] Masanae Koeda., “From Phantom Omni setup to Programming” URL https://vml.sakura.ne.jp/koeda/phantom/index.html (Accessed Dec 25, 2019)

[50] B. Siciliano and O. Khatib, Springer Handbook of Robotics, 2nd ed. Springer Publishing Company, Incorporated, 2016.

[51] J. Park and O. Khatib, “A haptic teleoperation approach based on contact force control,” The International Journal of Robotics Research, vol. 25, no. 5-6, pp. 575–591, may 2006.

[52] J. G. Wildenbeest, D. A. Abbink, C. J. Heemskerk, F. C. van der Helm, and H. Boessenkool, “The impact of haptic feedback quality on the performance of teleoperated assembly tasks,” IEEE Trans. Haptics, vol. 6, no. 2, pp. 242–252, Apr. 2013.

[53] J. Draper, W. Moore, J. Herndon, and B. Weil, “Effects of force reflection on servo manipulator task performance,” in Proc. Int. Topical Meet. Remote Syst. Robot. Hostile Environ., 1986.

[54] B. Hannaford, L. Wood, D. A. Mcaffee, and H. Zak, “Performance evaluation of a six-axis generalized force-reflecting teleoperator,” IEEE Trans. Syst., Man, Cybern., vol. 21, no. 3, pp. 620–633, May/Jun. 1991.

[55] Michael J. Tuttman., “Excavation Damage to Underground Utilities – Expert Article” URL https://www.robsonforensic.com/articles/underground-utilities-expert-witness (Accessed Dec 18, 2019)

[56] Michael J. Tuttman., “Excavation Damage to Underground Utilities” URL https://www.robsonforensic.com/articles/underground-utilities-expert-witness/ (Accessed Mar 9, 2020).

[57] W. Amaya, H. Yu, and M. Moreno, "Ux impacts of haptic latency in automotive interfaces," Immersion Corporation, Tech. Rep., 2013.